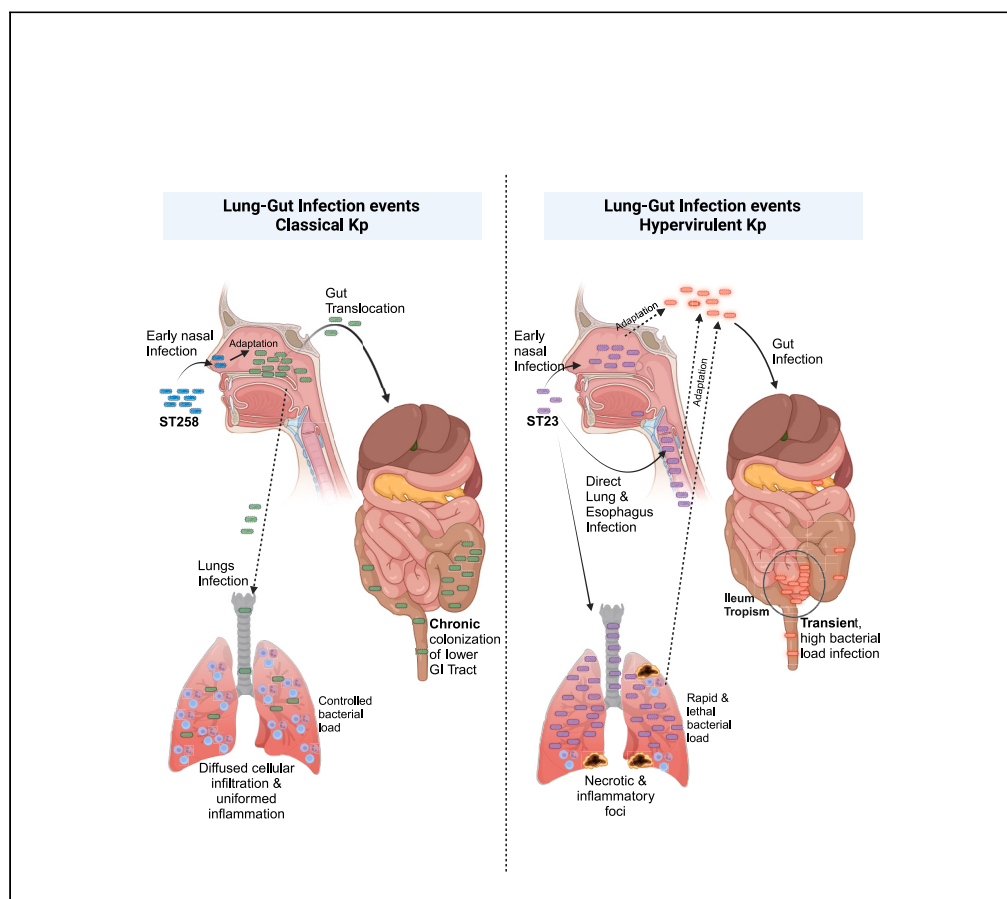


## Article

Differential mucosal tropism and dissemination of classical and hypervirulent *Klebsiella pneumoniae* infection

Teck-Hui Teo,  
Nurul N. Ayuni,  
Michelle Yin, ...,  
Barry N. Kreiswirth,  
Liang Chen, Pablo  
Bifani

teo\_teck\_hui@idlabs.a-star.  
edu.sg (T.-H.T.)  
pablo\_bifani@idlabs.a-star.edu.  
sg (P.B.)

**Highlights**

Classical *Klebsiella pneumoniae* (cKp) induces diffused lung inflammation

Hypervirulent *Klebsiella pneumoniae* (hvKp) induces necrotic lung inflammation

Early nasal infection is essential for cKp to establish chronic colonization of the gut

hvKp airway infection led to high but transient bacterial load in the ileum

## Article

Differential mucosal tropism and dissemination of classical and hypervirulent *Klebsiella pneumoniae* infection

Teck-Hui Teo,<sup>1,\*</sup> Nurul N. Ayuni,<sup>2</sup> Michelle Yin,<sup>1</sup> Jun Hao Liew,<sup>1,2</sup> Jason Q. Chen,<sup>1</sup> Natalia Kurepina,<sup>3</sup> Ravisankar Rajarethinam,<sup>4</sup> Barry N. Kreiswirth,<sup>3,6</sup> Liang Chen,<sup>3,6</sup> and Pablo Bifani<sup>1,2,5,6,7,\*</sup>

## SUMMARY

***Klebsiella pneumoniae* (Kp) infection is an important healthcare concern. The ST258 classical (c)Kp strain is dominant in hospital-acquired infections in North America and Europe, while ST23 hypervirulent (hv)Kp prevails in community-acquired infections in Asia. This study aimed to develop symptomatic mucosal infection models in mice that mirror natural infections in humans to gain a deeper understanding of Kp mucosal pathogenesis. We showed that cKp replicates in the nasal cavity instead of the lungs, and this early infection event is crucial for the establishment of chronic colonization in the cecum and colon. In contrast, hvKp replicates directly in the lungs to lethal bacterial load, and early infection of esophagus supported downstream transient colonization in the ileum and cecum. Here, we have developed an *in vivo* model that illuminates how differences in Kp tropism are responsible for virulence and disease phenotype in cKp and hvKp, providing the basis for further mechanistic study.**

## INTRODUCTION

Antimicrobial resistance (AMR) infections pose a significant global threat, with profound economic and public health consequences. Economically, the World Bank Group estimates that AMR could reduce GDP between 1.1% and 3.8%,<sup>1</sup> highlighting the magnitude of the economic burden. However, the most alarming concern is the public health impact. A recent report estimated that 4.95 million deaths were associated with AMR infections in 2019 alone, with *Escherichia coli*, *Staphylococcus aureus*, and *Klebsiella pneumoniae* (Kp) being the top mortality-causing pathogens.<sup>2</sup> Among them, Kp is responsible for the highest proportion of carbapenem-resistant infections, accounting for ~80% in the USA<sup>3</sup> and ~40% in Asia.<sup>4</sup> Unfortunately, available antibiotics are often ineffective against these infections, making Kp a critical priority bacterium in urgent need of new treatment, as classified by the World Health Organization (WHO).

Kp is a non-motile gram-negative bacterium belonging to the family of Enterobacteriaceae. It has been classified into classical (c) or hypervirulent (hv) subtype based on their pathotypes. The term “hypervirulent” was first introduced in the 1980s after an outbreak of liver abscess and complicated septic endophthalmitis in Taiwan caused by Kp.<sup>5</sup> However, our current understanding of the disease shows that classical and hypervirulent classifications extend beyond differences in the reported clinical phenotypes. They are also associated with specific geographical distribution, clonal group (CG) preference, antimicrobial resistance, and expression of virulence factors.<sup>6</sup> Specifically, cKp is endemic worldwide and is typically multidrug resistant and associated with hospital acquired infections (HAI). Among the HAI, cKp belonging to clonal group 258 (CG258) is the most prevalent globally, whereby sequence type (ST) 258 and ST512 are predominant in North America and Europe<sup>3,7,8</sup> and ST11 is predominant in China and Taiwan.<sup>9,10</sup> However, other parts of Asia with nationwide molecular epidemiology studies reported a highly varied STs among the cKp HAI without a clear predominant ST.<sup>11–13</sup>

On the other hand, hvKp is a significant concern in Asia, where community-acquired infections (CAIs) caused by hvKp are common. The endemicity of hvKp is currently limited to Asian countries,<sup>14–16</sup> with prevalent clones being CG23 (ST23, ST26, ST57, and ST163),<sup>17–22</sup> CG65 (ST65 and ST375), and CG86 (ST86).<sup>8,22,23</sup> Until now, most hvKp infection are drug-susceptible.<sup>24</sup> ST23 is the most predominant with a prevalence rate of 30%–85% among hvKp cases.<sup>17–22,25</sup> Importantly, sporadic cases of ST23 Kp have begun to emerge in different parts of Europe and North America,<sup>26–33</sup> highlighting the possibility of an expanding endemicity.

<sup>1</sup>Agency for Science, Technology and Research (A\*STAR), Infectious Diseases (ID) Labs, Singapore 429621, Singapore

<sup>2</sup>Infectious Diseases Translational Research Programme, Department of Microbiology and Immunology, Yong Loo Lin School of Medicine, National University of Singapore, Singapore 117545, Singapore

<sup>3</sup>Hackensack Meridian Health Center for Discovery and Innovation, Nutley, NJ 07110, USA

<sup>4</sup>Institute of Molecular and Cell Biology, Agency for Science, Technology and Research (A\*STAR), Singapore 138673, Singapore

<sup>5</sup>Department of Infection Biology, Faculty of Infectious and Tropical Diseases, London School of Hygiene and Tropical Medicine, London WC1E7HT, UK

<sup>6</sup>Senior author

<sup>7</sup>Lead contact

\*Correspondence: [teo\\_teck\\_hui@idlabs.a-star.edu.sg](mailto:teo_teck_hui@idlabs.a-star.edu.sg) (T.-H.T.), [pablo\\_bifani@idlabs.a-star.edu.sg](mailto:pablo_bifani@idlabs.a-star.edu.sg) (P.B.)  
<https://doi.org/10.1016/j.isci.2024.108875>



The current state of Kp research has shown a bias toward cKp, with a greater emphasis placed on the AMR nature of this strain type from a public health perspective. This is because most hvKp remains treatable with existing antibiotics.<sup>24</sup> However, there are growing concerns regarding the convergence of AMR and hypervirulence in Kp, which is mediated by virulence or resistance gene horizontal transfer.<sup>11,34–36</sup> This presents a significant risk of outbreaks with AMR hvKp that are both pathologically aggressive and difficult to treat.

Despite the increasing prevalence of Kp, the mechanism of pathogenesis remains elusive for both cKp and hvKp. Our study aims to elucidate mechanism of Kp tropism and pathogenesis that differentiate cKp and hvKp at the mucosal interface. We postulate that the host mucosal surface is a critical entry point of the pathogen and likely determinant of diseases progression. Better understanding of the onset of infection and pathogenicity will allow for better prediction of disease progression and outcome. Specifically, Kp commonly induced pneumonia and urinary tract infection, both of which are associated with the mucosal system. In addition, Kp has been shown to colonize the nasopharynx and gastrointestinal tract of asymptomatic carriers,<sup>37–40</sup> and the development of clinical disease has shown to be linked to colonization.<sup>41</sup> However, the sequence of events that leads to the establishment of infection or progression to complications in different mucosal membranes remain poorly defined. Existing studies have mainly focused on genetic profiling of bacterial virulence factors and have not adequately addressed this gap. Currently, there are no standard animal models of Kp infection that accurately mimic the clinical disease. Additionally, there are no models of gastrointestinal colonization that display detectable cKp without prior antibiotic treatment or artificial pre-treatment with sodium bicarbonate.<sup>42</sup> Therefore, there is an urgent need for an *in vivo* system that can accurately model Kp infection in mucosal membranes that provides the complexity of host-pathogen interactions.

In this study, we hypothesize that cKp and hvKp present distinct mucosal tropisms, which may determine their differential propensities to induce disease complications or establish chronic colonization. To investigate this, we selected the most prevalent ST258 in the USA and ST23 in Asia as the representative cKp and hvKp clones and established pathogenic ST258 and ST23 mucosal infection models that do not require antibiotic pre-treatment or invasive inoculation method. We used these models to define bacterial tropism, dissemination, and lung pathology. This will provide insight into the differences in mucosal pathogenesis of cKp and hvKp, which play a crucial role in disease pathogenicity and may explain the distinction in clinical manifestations observed between these two dominant Kp clonal groups.

## RESULTS

### Early nasal cavity tropism hastens establishment of pathogenic respiratory tract by Kp

Early clinical surveillance reports have showed that Kp could colonize nasopharyngeal region,<sup>37,39,40</sup> suggesting a possible role of the nasal cavity as an entry point or Kp reservoir in humans. However, most animal studies with Kp only focused on the lungs,<sup>42</sup> while the upper respiratory tracts are largely neglected. To define the role of the nasal cavity in infection, we optimized the standard intranasal and intratracheal infection. We first used trypan blue inoculation as a means to measure inoculum delivery into the airways and lungs. Both intranasal and intratracheal inoculations delivered similar amount of inoculum into the lungs (Figure S1A), but intranasal inoculation delivered a greater amount of inoculum directly into the nasal cavity and nasopharynx opening at the point of inoculation (Figure S1B). This provides a basis for attributing a role to the nasal cavity by comparing infection outcomes between these two methods.

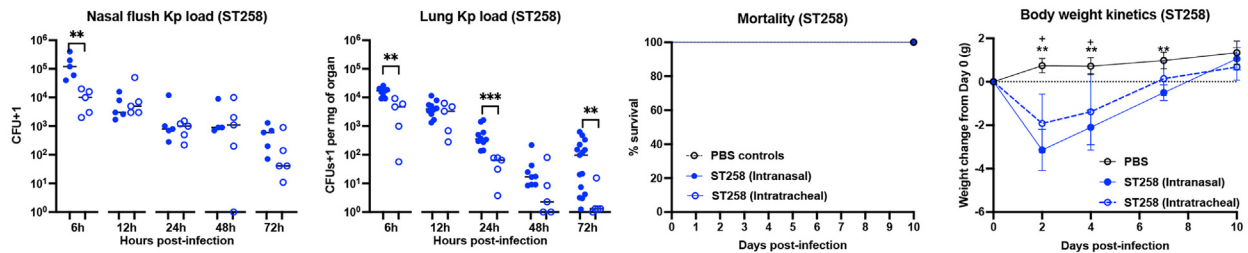
We next established pathogenic respiratory tract infections of cKp and hvKp using both the intranasal and intratracheal inoculation methods. We focused our study models on ST258 and ST23 for cKp and hvKp, respectively, because ST258 is the dominant Kp for HAIs in the USA and Europe,<sup>3,7,8</sup> while ST23 is the dominant CAIs Kp in Asia.<sup>17–22</sup> Using a representative ST258 cKp from the USA (Kp1085;  $6 \times 10^7$  CFU inoculum), we profiled the kinetics of Kp load in the lung and nasal flush, mortality, and weight loss as disease readouts (Figure 1A). In the intranasally infected mice, a higher initial Kp load in the nasal cavity at 6h is associated with a higher bacterial load in the lungs during later phase of the infection at 24h and 72h (Figure 1A). In the intratracheally infected mice, the nasal bacterial load rapidly increased to similar peak levels as intranasal infection by 12h. A closer examination showed that cKp bacterial load during acute infection remains fairly stable in the nasal cavity but rapidly wanes within the lungs in both methods of infection (Figures 1A–1C and 1D). No mortality was observed by intranasal or intratracheal cKp infection and mice displayed similar degree of weight loss in the first 7 days post-infection (Figure 1A).

To establish similar respiratory tract hvKp infection models with a representative ST23 hvKp isolate from Singapore (KpEC0675), we had to reduce infection dosage to  $1 \times 10^3$  CFU to avoid acute lethality. Higher dosage from  $1 \times 10^4$  CFU led to mortality by two days post-infection, which was too rapid for meaningful analysis (data not shown). A similar set-up based on pathogenicity but not infection dose for comparative study has been used in Wong et al.<sup>43</sup> where hvKp dosage was adjusted to be 2-Logs lower than cKp. In intranasally infected mice, the higher initial nasal hvKp from 6h post-infection hastened disease development as demonstrated by a higher lung Kp load at 6h and 12h, and marginally earlier mortality at day 3–4 as compared to intratracheally infected mice (Figure 1B). In the hvKp intratracheally infected mice, rapid bacterial replication occurs in the nasal cavity and peaks at similar levels by 24h as intranasally infected mice (Figure 1B). Unlike cKp where bacterial load wane as infection progress to 72h, hvKp load in the nasal flush was stably maintained throughout the follow-up period (Figures 1A and 1B). Importantly, regardless of the inoculation methods, hvKp could replicate exponentially in the lungs from 12h onwards to a lethal bacterial load of  $>10^7$  CFU/mg tissue by 48h post-infection, leading to severe sign of illness such as weight loss, weakness, ruffled fur, convulsion, and eventual mortality (Figure 1B).

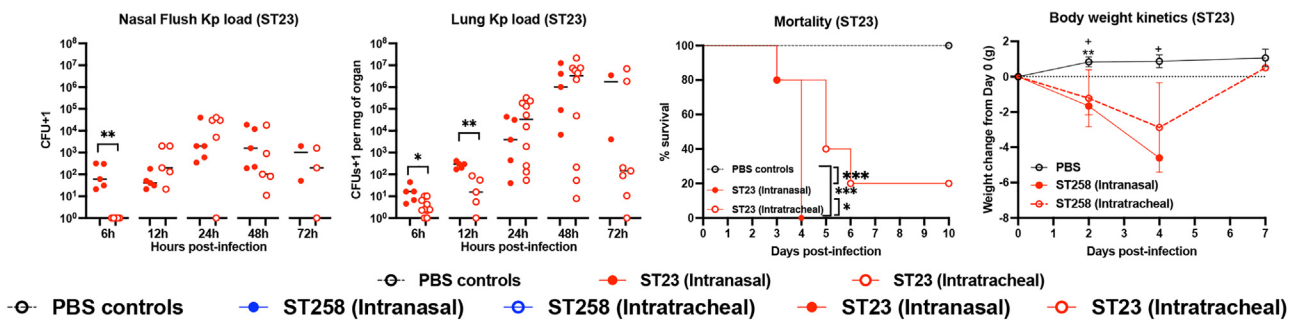
With the establishment of airway infection models using these two representative isolates, unless the use of other isolates is explicitly stated, all downstream cKp and hvKp infections will refer to ST258-Kp1085 and ST23-KpEC0675 isolates given at  $6 \times 10^7$  CFU and  $1 \times 10^3$  CFU, respectively.

To quantitatively assess the differences in the trend of bacterial replication and tropism between cKp and hvKp, we expressed the Kp load in the nasal flush and lungs as a ratio of the initial bacterial inoculum (Figures 1C and 1D). As expected, cKp displayed a waning bacterial

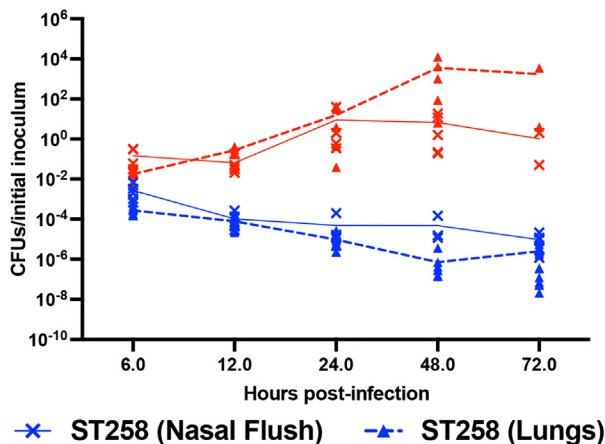
**A** Classical Kp



**B** Hypervirulent Kp



**C** Kp replication in respiratory tract (intranasal)



**D** Kp replication in respiratory tract (intratracheal)

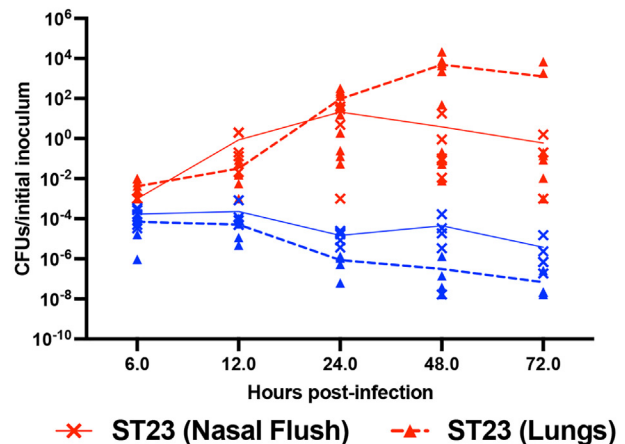


**Figure 1. Differential classical and hypervirulent Kp tropism in the nasal cavity and lungs**

(A) Kinetics of Kp load in the nasal flush and lungs, mortality and body weight changes in mice infected with ST258-Kp1085 ( $6 \times 10^7$  CFU) intranasally or intratracheally ( $n \geq 5$  per group).

(B) Kinetics of Kp load in the nasal flush and lungs, mortality and body weight changes in mice infected with ST23-KpEC0675 ( $1 \times 10^3$  CFU) intranasally or intratracheally ( $n \geq 5$  per group). Data points in 72h are less than 5 due to mortality prior to harvest. Ratio of Kp load in the nasal flush and lungs relative to the initial inoculum in mice infected (C) intranasally or (D) intratracheally with ST258 or ST23 ( $n \geq 5$  per group).

Body weight kinetics were presented as mean  $\pm$  SD and analyzed by Kruskal-Wallis with Dunn's multiple comparison test (PBS vs. Intranasal represented by \* $p < 0.05$  and \*\* $p < 0.01$ ; PBS vs. intratracheal represented by + $p < 0.05$ ). Mortality data were analyzed with Log rank (Mantel-Cox) test (\* $p < 0.05$ ; \*\*\* $p < 0.001$ ). All paired wise comparisons were analyzed by Mann-Whitney 2-tailed analysis (\* $p < 0.05$ ; \*\*\* $p < 0.001$ ). Each point in the dot plot corresponds to data from 1 mouse. Data shown in each panel are pooled from at least 3 independent experiments.

replication in both nasal flush and lungs as infection progresses. A greater proportion of bacteria were found in the nasal cavity (Figures 1C and 1D). By contrast, bacterial replication in both the nasal flush and lungs increases as hvKp infection progressed, and a greater proportion of the bacteria were distributed in the lungs (Figures 1C and 1D). The same trend was observed for both methods of inoculation (Figures 1C and 1D).

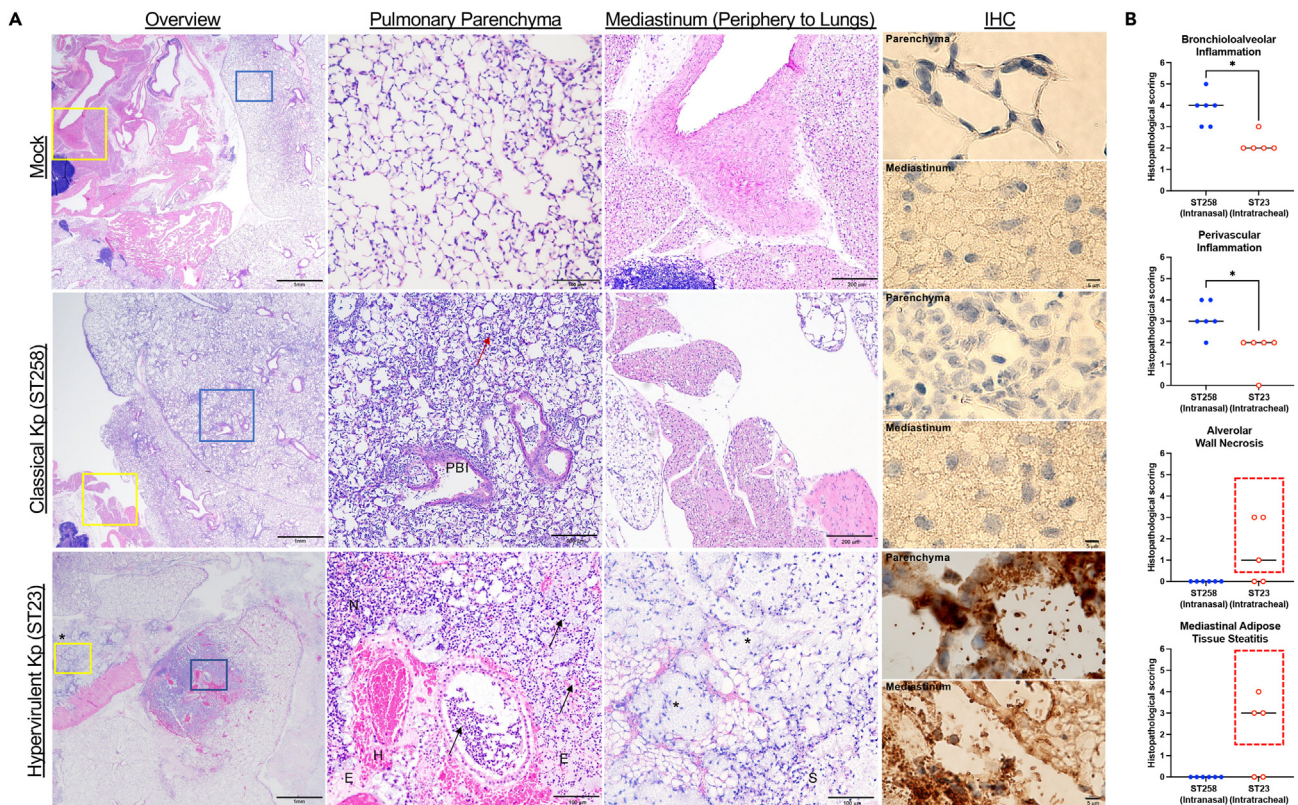


**Figure 2. Differential Kp tropism and pathology in the lungs of cKp and hvKp infected mice**

(A) Representative H&E and immunohistochemistry (IHC) images of PBS (n = 3), ST258 (n = 6), and ST23 (n = 5) infected mice at 48hpi. Pulmonary parenchyma and mediastinum regions are indicated with blue and yellow box respectively at low magnification. Representative IHC images of pulmonary parenchyma and mediastinum were taken at high magnification and Kp staining is identified as brown rod-shaped cells. “Red arrow”: Infiltration of neutrophils into alveolar sac and bronchioles, “Black arrow”: necrotizing bronchopneumonia, \*: region of massive bacterial spread into the mediastinal area, “N”: necrosis, “E”: edema, “H”: perivascular hemorrhages and “S”: steatitis.

(B) Histological scoring of differentiating lung phenotypes of ST258 (n = 6) and ST23 (n = 5) infected mice at 48hpi. Data were analyzed by Mann-Whitney 2-tailed analysis (\*p < 0.05). Mice that displayed detectable Kp in the lung parenchyma or mediastinal adipose tissues were highlighted with dotted red box. ST258 infection was induced with Kp1085 ( $6 \times 10^7$ CFU) intranasally. ST23 infection was done with KpEC0675 ( $1 \times 10^3$ CFU) intratracheally.

Taken together, the nasal cavity appears to facilitate the initial infection of both cKp and hvKp. However, cKp displayed a greater tropism for the nasal cavity over the lungs, while hvKp showed a greater tropism for the lungs over the nasal cavity.

### cKp and hvKp induce distinct histopathology in the lungs

To understand how the differential tropism of cKp and hvKp within the respiratory tract influenced the nature of the lung pathology, we performed histopathological assessment of mice lungs using H&E staining on day two post-infection. We selected 48h samples from intranasally ST258-infected mice because infection and bacterial load in the lungs were consistent (Figure 1A). In contrast, intratracheal infection was selected for ST23 because a 20%–40% mortality was observed in the intranasal group at harvest time point, while all intratracheal infected mice survived. Selecting intranasal ST23-infected mice at this time point skews the data toward the less severe mice in the group.

In the cKp infected lungs, we observed neutrophils infiltration into pulmonary parenchyma of the alveolar sac and alveolar septum, causing degeneration of neutrophils and cellular debris. Similar inflammatory phenotypes are also present at the perivascular and peribronchiolar area. (Figure S2). This type of suppurative inflammation is often accompanied with the presence of macrophages, fibrin deposition, and rarely with intra alveolar hemorrhages. Despite such widespread pulmonary inflammation, surprisingly, bacilli were absent within the lung, suggesting other possible host mediated pathology that requires further investigation (Figure 2A-IHC; Figure S2). Periphery of lung parenchyma is mostly unaffected.

Conversely, lesions induced by hvKp in mice lungs were confined to the lung periphery and displays severe damage. The damaged regions are associated with the presence of bacilli, necrotizing bronchopneumonia, and hemorrhages (Figure 2). Widening of perivascular area, which constricts pulmonary blood vessel, was observed and accompanied by compression of the adjacent alveoli in hvKp infected mice lungs (Figure S2). However, when the entire lung section is considered, the overall score of inflammation at bronchioalveolar and perivascular regions is lower in this group as compared to cKp treated mice (Figure 2B).

Interestingly, adjoining mediastinal region to these necrotizing foci in hvKp-infected mice displays inflammation of adipose tissue, steatitis, along with bacterial infiltration (Figure 2A). This suggests that tissue necrosis at the periphery of the lung parenchyma could facilitate the spread of hvKp into the mediastinal region. Subsequently, the hvKp replicates to high bacterial loads within the mediastinal region that was profiled in the isolated lungs at day two post-infection (Figure 1B). In contrast, cKp infected mice displayed healthy mediastinal adipose tissue with the complete absence of bacilli (Figure 2A).

### Lungs and nasal cavity tropism in different ST258 cKp and ST23 hvKp

Next, we tested if the tropism in the lungs and nasal cavity is reproduced in other Kp isolates within ST258 and ST23. For cKp, in addition to the reference cKp1085, we selected five more USA isolates within ST258 (Kp1050, Kp1085, Kp1055, Kp1054, and Kp1064) belonging to K-locus (KL) 107, 23, and 106, respectively (Table S1). For hvKp, in addition to the reference KpEC0675, we selected 2 additional Singapore ST23-KL1 isolates (KpSGH10 and KpNUH27) (Table S1). WGS analysis revealed that the three ST23 hvKp strains carry virulence genes encoding yersiniabactin, colibactin, aerobactin, and salmochelin. KpEC0675, SGH10, and KpNUH27 all harbor wild-type mucoid phenotype regulator gene *rmpA*, *rmpC*, and mucoid phenotype synthesis gene *rmpD*. In addition, the three hvKp also harbor a truncated *rmpA2* gene. In contrast, only two cKp ST258 strains (Kp1050 and Kp1085) carry genes encoding yersiniabactin and colibactin, but they were negative for all the other virulence genes detected in the hvKp ST23 strains (Figure 3A; Table S1). The ST258 strains and the ST23 strain KpEC0675 also harbor carbapenemase gene *bla<sub>KPC</sub>* (–2 or –3) (Table S1).

Phylogenetic analysis of the five ST258 against a collection of completely sequenced ST258 strains in GenBank RefSeq database showed that the five ST258 strains belong to three different genetic clusters. Phylogenetic analysis also revealed that the three ST23 strains belonged to a large cluster (corresponding to CG23-1 in a previous study<sup>44</sup>) but weren't directly related. Core SNP analysis indicated the three hvKp strains differed by an average 314 core SNPs (range 213–369).

To show that the genotypic differences in the mucoid regulator translate into phenotypic differences, we performed a sedimentation assay to determine the mucoviscosity of the capsule<sup>45</sup> (Figures 4A and 4B). In this assay, the degree of mucoviscosity corresponds to the quantity of bacteria that fails to pellet with the sedimentation spin.<sup>45</sup> Expectedly, all the hypervirulent ST23 Kp displayed a greater degree of mucoviscosity than classical ST258 Kp (Figures 4A and 4B).

We next proceed to characterize these different ST258 and ST23 Kp by *in vivo* infection. Since a more consistent infection outcome is obtained by intranasal infection (Figure 1), these different isolates were tested by intranasal infection. As expected, all cKp isolates of ST258 displayed a higher tropism for the nasal cavity than the lungs at day 2 post-infection (Figure 4C). While the bacterial load in the nasal flush was similar across the different ST258 cKp, higher lung Kp load (~10x) were seen in cKp in KL106 cKp as compared to KL23 and KL107 ST258 cKp (Figure 4C). All ST258 cKp infected mice were relatively healthy based on behavioral observation at the point of harvest. In contrast, all ST23 hvKp infected mice at day two post-infection displayed pronounced weakness at the point of harvest. Importantly, the Kp load in the nasal cavity of the ST23 isolates was similar to the ST258 isolates but bacterial dissemination in the respiratory tract skewed toward the lungs and not the nasal cavity (Figure 4D). KpNUH27 is associated with a lower lung bacterial load with no impact on the nasal bacterial load (Figure 4C). A closer examination of the WGS in the 3 ST23 suggested that this waned phenotype in KpNUH27 could be associated with a ISKpn74 (IS5 family) insertion at 564 bp upstream of O-antigen synthesis *wb* gene cluster (Figure 3A; Table S1). Overall, these data showed that the differential tropism into the nasal cavity and lungs was reproducible across the different ST258 and ST23 isolates.

### cKp and hvKp display differential gut colonization profiles

We next profiled whether pathogenic airway infection with either cKp or hvKp leads to gut colonization. Specifically, gut colonization by Kp has been shown to be associated with hospital acquired infections,<sup>41,46</sup> hence the *in vivo* modeling of gut colonization could provide important information on the spread of Kp, particularly in a nosocomial environment.

To understand the kinetics of the bacterial load in the gut, fecal Kp were monitored. Similar to reports of silent chronic colonization of humans with cKp,<sup>47</sup> detectable fecal bacterial load was seen in the cKp infected mice for as long as 70 days (Figure 5A), where experiments were terminated. No signs of illness were identified by physical examination from one-week post-infection onwards. Strikingly, intranasal infection with cKp induced a higher level of late stage fecal Kp load (from day 21 onwards) compared to intratracheal infection, and this is associated with a higher cumulative Kp burden in the GI tract (stomach to colon) at 72h post-infection (Figure 5A). A higher proportion of successful chronic gut colonization was also observed in intranasal cKp infected mice (100%) compared to intratracheal infected mice (60%) at day 70 of the follow-up (Figure 5A; Figure S3). No bacteria were detected in the nasal flush or lungs of all cKp infected mice at day 70 (Figure S3). Conversely, airway hvKp infection induced high levels of acute Kp load (day 2) in the feces (Figure 5B). However, in the small proportion of mice (10–20%) that survived the infection, their fecal Kp load was rapidly resolved by day 7 post-infection (Figure 5B). Similar fecal Kp and GI tract Kp profile was seen in intranasal and intratracheal hvKp infected mice.

To understand if there are differences in the tropism along the different parts of the GI tract for cKp and hvKp, we profiled the bacterial load in the stomach, duodenum, jejunum, ileum, cecum, and colon (Figures 5C and 5D; Figure S3; S4). In all cKp infected mice, most of the bacteria colonize the cecum during both acute (Figures 5C and 5D) and chronic (Figure S3) phase of the disease. Concordant with the fecal Kp load (Figure 5A), intranasally infected cKp mice also displayed higher cecum bacterial load than intratracheally infected mice at 12h, 72h and day 70 post-infection (Figure 5D; Figure S3). No bacteria was detected in the lungs or the nasal flush of all cKp infected mice at day 70 post-infection (Figure S3), suggesting that the gut but not the respiratory tract provides the niche for chronic cKp colonization.

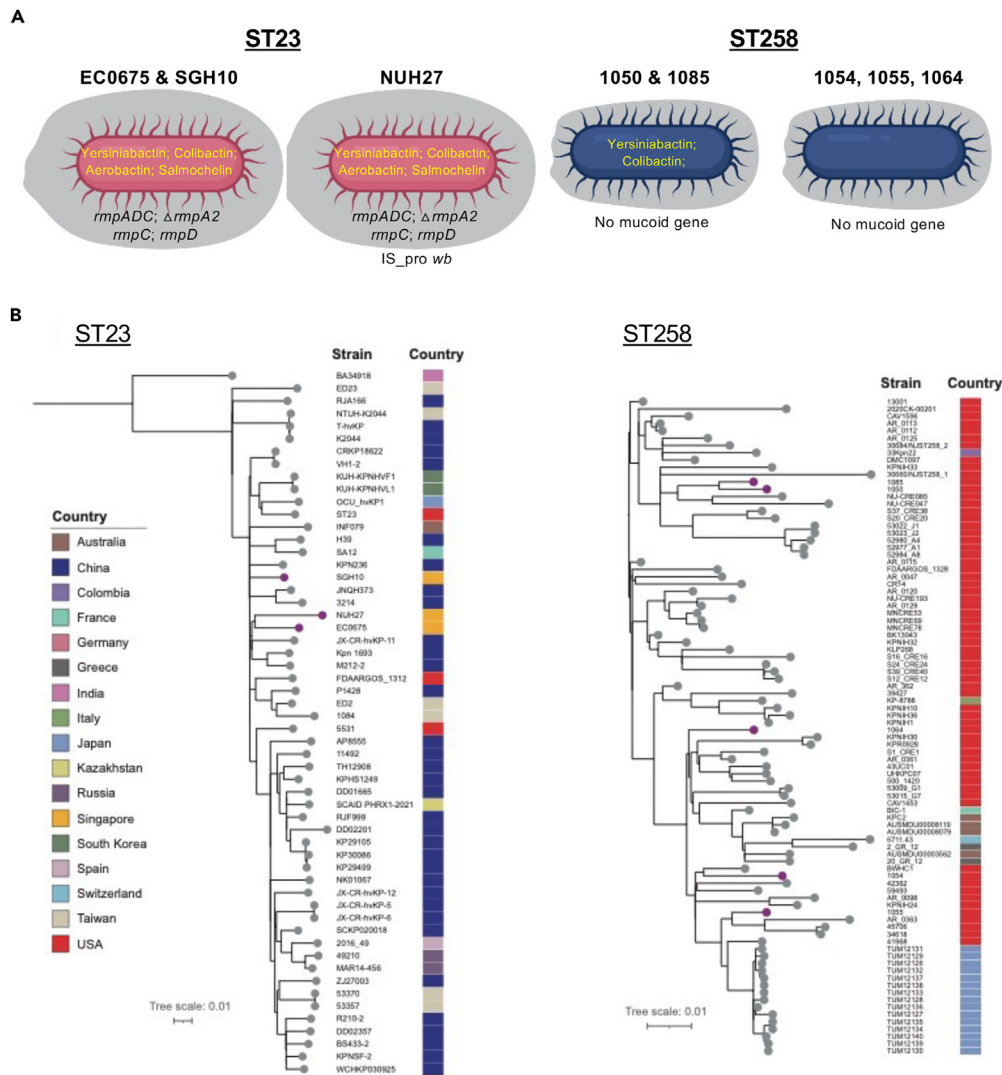


**Figure 3. Genomic analysis of different Kp in ST258 and ST23**

(A) Diagram representation of virulence genes of different Kp used in this study. ST23: KpEC0675, KPNSGH10, KPNUH27, and ST258: Kp1050, KP1054, Kp1055, Kp1064, and Kp1085. The grayscale highlights represent capsule regulated by *rmpADC* and *rmpA2* genotypes. Siderophore genotype was indicated in the bacterial diagram. An extra ISKpn74 insertion at 654bp upstream of O-antigen synthesis *wb* gene cluster in NUH27 is highlighted by IS<sub>pro</sub> wb.

(B) Core snp phylogenetic analysis of Kp used in this study against completely closed genomes in the NCBI RefSeq database (accessed on 3/15/2023). The color bar denotes the countries of the isolates. Purple nodes indicate the strains used in this study.

In hvKp infected mice, a higher proportion of bacteria colonizes the small intestine at the ileum by 48h post-infection with an exponential increase in gut bacterial load (Figures 5B–5D). Similar Kp load in the different parts of the GI tract was seen for intranasal and intratracheal hvKp infection from 6h–72h post-infection (Figure 5D; Figure S4B). However, the relative proportion of Kp along the GI tract in the intranasal hvKp infected mice shifted from the ileum to the cecum at 72h post-infection (Figure 5C).

Taken together, a high initial inoculum of cKp infection in the nasal cavity by the intranasal route promoted a higher chronic bacterial load in the gut that primarily resides in the cecum. In hvKp infection, the method of airway infection does not influence the gut colonization or gut bacterial load. Unlike cKp, higher ileum tropism for hvKp is observed and gut colonization is transient when mice recover from the lung infection.

Intranasal infection successfully reproduces gut colonization profile with different ST258 cKp and ST23 hvKp without antibiotic pre-treatment.

To demonstrate that the colonization of the gut by cKp and hvKp is not limited to a single isolate of ST258 and ST23, we profiled the cecum Kp load at day 2 post-infection using the same list of different ST258 cKp and ST23 hvKp tested in Figures 3 and 4. Expectedly, intranasal infection induced colonization of Kp in the cecum for both cKp and hvKp without the need of antibiotic pre-treatment (Figure S5). Within the ST258, KL106 Kp induced at higher bacterial load (~10x) than KL23 and KL107 in the cecum (Figure S5A). Interestingly, the diminished

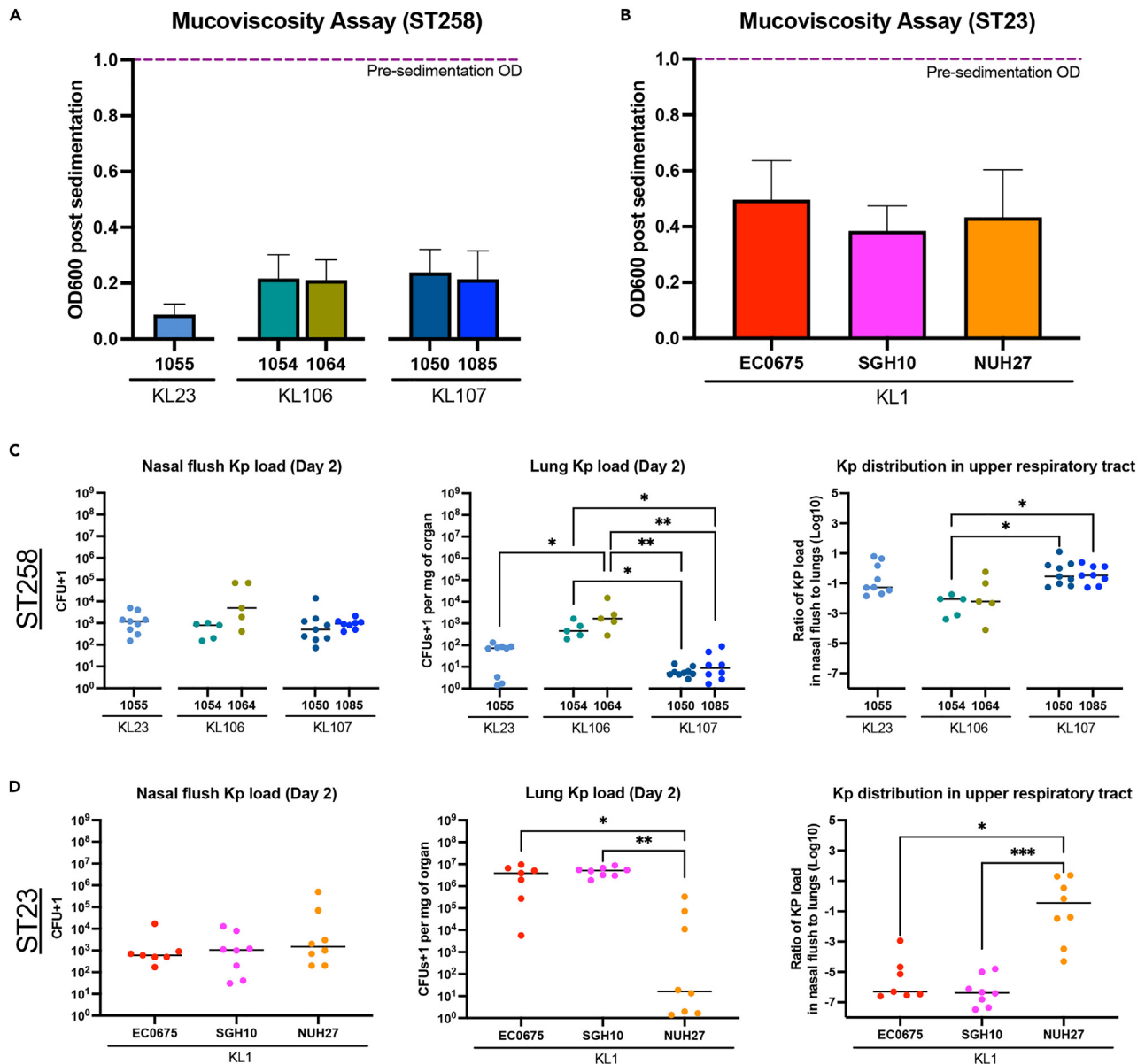


**Figure 4. Kp distribution in the respiratory tract predicts hypervirulence**

Mucoviscosity assay of the different Kp from (A) ST258 and (B) ST23. All bacteria were adjusted to OD1 prior to sedimentation spin. OD600 reading of the supernatant post-sedimentation is a measure of mucoviscosity. Data were presented as mean + SD. Data from 4 biological replicates were presented.

(C) Kp load in the nasal cavity and lungs of mice infected intranasally with different classical cKp belonging to ST258 from KL23, KL106 and KL107.

(D) Kp load in the nasal cavity and lungs of mice infected intranasally with different classical hvKp belonging to ST23 in KL1. Bacterial load in the nasal cavity is expressed as a ratio to the lungs as a measurement of Kp distribution in the upper respiratory tract. Data shown in (C) and (D) were pooled from 2 independent experiments and each data point correspond to 1 mouse. Data were analyzed by Kruskal-Wallis test with Dunn's multiple comparison (\*p < 0.05; \*\*p < 0.01) All classical and hypervirulent Kp infection was performed at  $6 \times 10^7$  CFU and  $1 \times 10^3$  CFU respectively.

lung KpNUH27 load is also associated with a lower cecum bacterial load ( $\sim 10$ x) in the ST23 infected mice (Figure S5B). Similar to the cecum data from our reference ST258 and ST23 isolates (Figure 5D), except for KpNUH27, the other hvKp infected mice display a cecum Kp load that is  $\sim 10$ – $100$ x higher than cKp infected mice (Figure S5).

### Early transient nasal cavity infection establishes cKp colonization in the gut

We next tested whether airway infection is essential, or a straightforward fecal-oral route is sufficient to establish gut colonization by Kp. Previous reports suggested that oral cavity infection supports establishment of Kp colonization,<sup>48</sup> as such, we devised three modes of oral

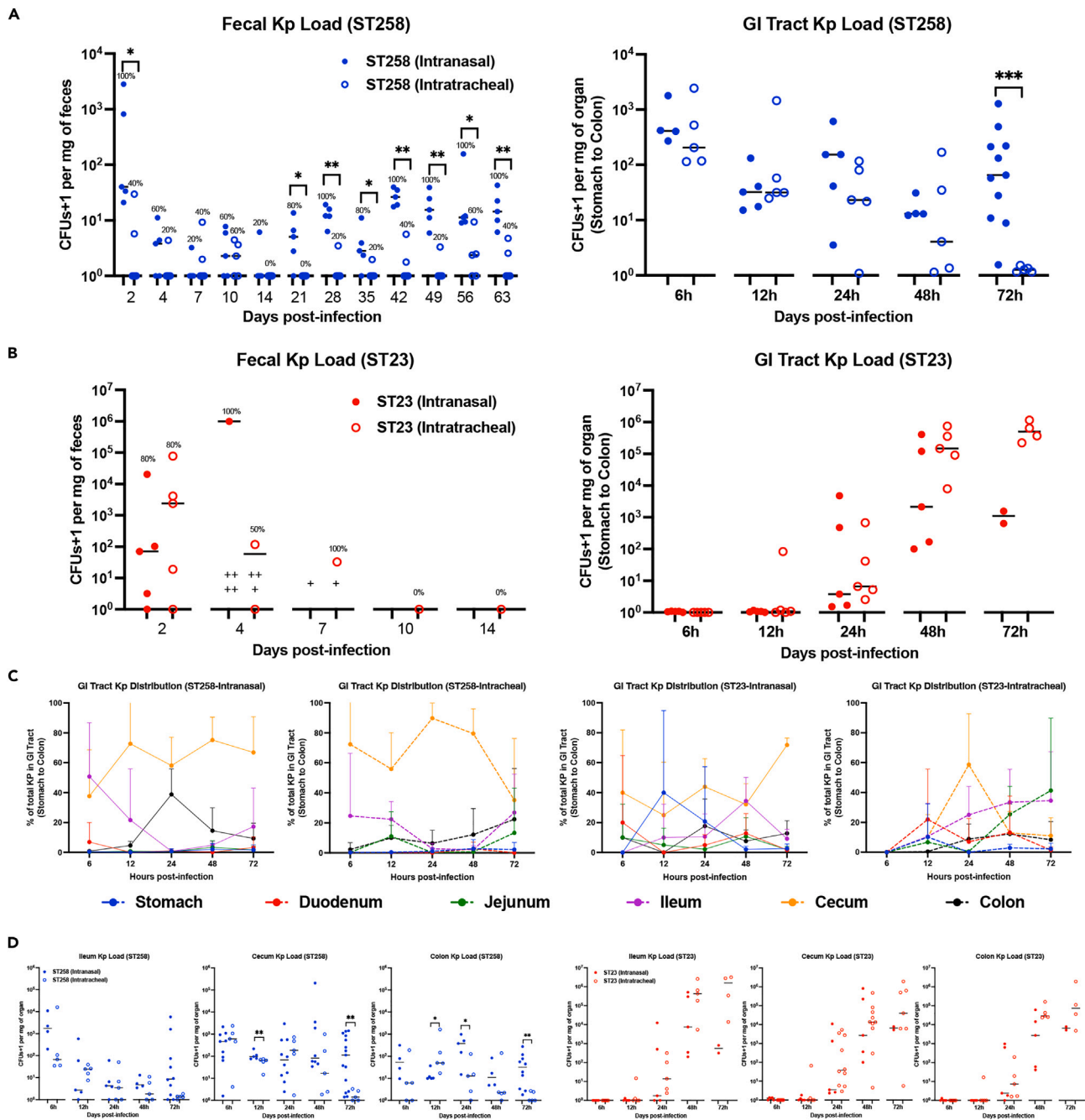


**Figure 5. Gut dissemination in airway infected *Klebsiella pneumoniae* mouse models**

Kinetics of fecal and gastrointestinal tract (GI) Kp load in intranasally or intratracheally (A) ST258-Kp1085 and (B) ST23-KpEC0675 infected mice ( $n \geq 5$  per group). "+" represent mice that died from infection before feces collection. The % of animal in the group that displayed fecal bacterial load above detection limit is indicated in the graph. Detection limit for fecal bacterial load is 100 CFUs in each collection prior to normalization by weight. Samples that fall below the detection limit are plotted along the x axis. GI tract Kp load is the cumulative bacterial load in stomach, duodenum, jejunum, ileum, cecum, and colon.

(C) Distribution of Kp load along different parts of the GI tract (Stomach to colon) in intranasally or intratracheally infected mice at 6, 12, 24, 48, and 72 hpi ( $n = 5$  per time-point).

(D) Ileum, cecum, and colon Kp load in intranasally or intratracheally infected mice at 6, 12, 24, 48, and 72 hpi. All paired wise comparisons were analyzed by Mann-Whitney 2-tailed analysis (\* $p < 0.05$ ; \*\* $p < 0.01$ ). Each data point from the dot plots is collected from 1 mouse.

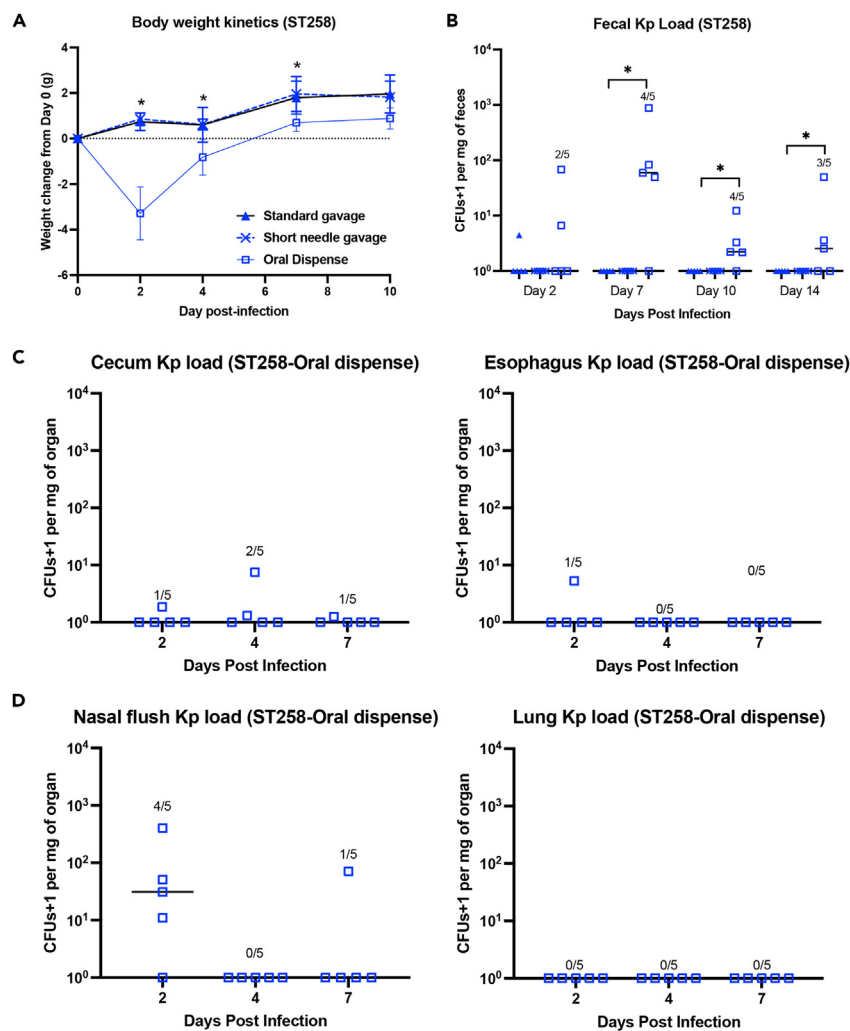


**Figure 6. Gut colonization through oral disperse of classical Kp is preceded by infection of the nasal cavity and not the lung**

(A) Body weight kinetics and (B) fecal Kp load in mice infected with ST258-Kp1085 ( $6 \times 10^7$  CFU) by standard oral gavage, short needle gavage and oral disperse ( $n \geq 5$  per group). Body weight kinetics were presented as mean  $\pm$  SD. Standard gavage group was assigned as controls and respective groups were compared against the controls using Kruskal-Wallis test with Dunn's multiple comparison ( $*p < 0.05$ ). Kp load in the (C) cecum, esophagus and (D) nasal flush, lungs of mice infected with ST258-Kp1085 by oral disperse ( $n \geq 5$  per group). Fraction of positive bacterial detection is given above the data points for all oral disperse infection in the different organs and fecal samples. Each point in the dot plot corresponds to data from 1 mouse.

infection that introduce the inoculum at different entry point of the upper GI tract (Figure S6). Specifically, standard gavage delivers inoculum just above the stomach, and short needle gavage delivers inoculum at the midpoint of the esophagus, while oral disperse delivers the inoculum to the mouth that will come into contact with the nasopharynx opening that connects to the nasal cavity (Figure S6).

Interestingly, only oral disperse but not the other two methods established gut colonization of cKp. Specifically, only oral disperse of cKp led to early weight loss in mice from day two post-infection, whereby recovery was observed by day 10 post-infection (Figure 6A). In addition, 40% of these mice had low dose of fecal Kp load at day two post-infection that peaked on day seven post-infection, with 80% displaying detectable fecal Kp (Figure 6B). Both standard gavage and short needle gavage failed to establish cKp colonization (Figures 6A and 6B). Further examination of the nasal cavity, lungs, esophagus (upper GI tract) and cecum of the mice infected with cKp by oral disperse showed that transient peak of nasal Kp at day two post-infection preceded the detection of Kp in the cecum and feces (Figures 6B–6D). In addition, when present, the bacterial load in the nasal flush was  $\sim 10$ – $100$ x higher than the cecum Kp load (Figures 6C and 6D). Unlike intranasal infection, a longer time is required to establish gut colonization in oral disperse mice and the established colonization existed at lower bacterial load based on cecum Kp quantification (Figures 5D and 6C). No bacteria were detected in the lungs, while only one out five mice displayed low levels of Kp in the esophagus at day two post-infection (Figures 6C and 6D). These observations suggest that faecal-oral ingestion of cKp first infects the nasopharynx opening to spread into the nasal cavity, and this transient upper airway infection is essential for eventual dissemination of cKp into the gut.

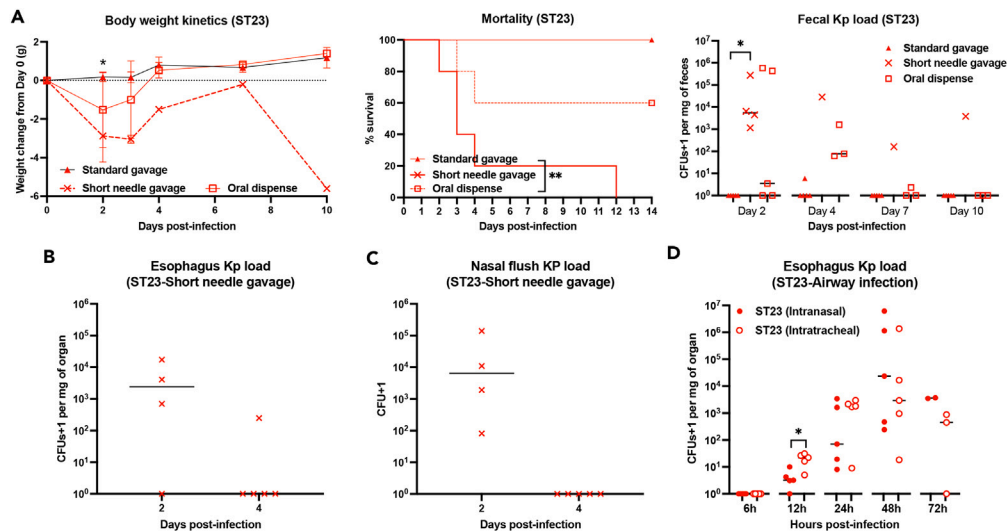


**Figure 7. Early esophagus infection by hypervirulent Kp induce high bacterial load of gastrointestinal bacterial load and mortality**

(A) Body weight kinetics, mortality and kinetics of fecal Kp load in mice infected with ST23-KpEC0675 ( $2 \times 10^6$  CFU) by standard oral gavage, short needle gavage and oral dispense ( $n \geq 5$  per group). Data of body weight kinetics were presented as mean  $\pm$  SD. Standard gavage group was assigned as controls and respective groups were compared against the controls using Kruskal-Wallis test with Dunn's multiple comparison (Standard gavage vs. short needle gavage:  $*p < 0.05$ ). Mortality data were analyzed with Log rank (Mantel-Cox) test ( $**p < 0.01$ ). Kp load in the (B) esophagus and (C) nasal flush of mice infected with ST23-KpEC0675 ( $2 \times 10^6$  CFU) by short needle gavage ( $n \geq 4$  per group) at day 2 and day 4 post-infection. (D) Kp load in the esophagus of mice infected intranasally or intratracheally with ST23-KpEC0675 ( $1 \times 10^3$  CFU). Paired wise comparisons were analyzed by Mann-Whitney 2-tailed analysis ( $*p < 0.05$ ). Each point in the dot plot corresponds to data from 1 mouse.

### hvKp utilizes esophagus infection to establish downstream intestinal colonization

We next performed the same type of oral infection methods using hvKp using similar dose ( $1 \times 10^3$  CFU) as the airway infection methods. Except for 1 mouse from the short needle gavage group that showed detectable Kp in the feces at day 7 post-infection, Kp colonization was not established in the rest of the mice (Figure S7).

We hypothesize that gut colonization in airway infected mice occurs through high bacterial load of Kp that enters the gut by mucociliary clearance from the airway as suggested by the exponential increase of lung Kp (Figure 1B) that preceded bacterial load increase in the gut (Figure 5B). To show that a higher bacterial load of infection dose could establish hvKp colonization through the different oral ingestion routes, we increased the infection dosage to  $2 \times 10^6$  CFU. Surprisingly, hvKp colonization in the gut was best established in the short needle gavage but not the other two methods with this increased infection dosage (Figure 7A). Specifically, lethal hvKp infection was established in 100% of short needle gavage mice with high fecal Kp load at day two post-infection (Figure 7A). Interestingly, standard gavage that delivers the bacteria into the stomach failed to establish gut colonization and fecal Kp was not detected in the mice across the different time-points (Figure 7A). Oral dispense only gave intermediate phenotype where gut infection was established in 60% of the mice with 40% mortality (Figure 7A). This outcome suggested that esophagus infection at the point of inoculation in short needle gavage setting could have supported establishment of downstream gut colonization.

To further define the role of esophagus in hvKp infection, we measured the Kp load in the esophagus of mice infected with hvKp via three different infection methods that consistently induced gut colonization, namely short needle gavage (Figure 7A), intranasal, and intratracheal infection (Figure 5B). Similar to intranasal or intratracheal infection (Figure 5C; Figure S4), short needle gavage of hvKp induced a high Kp load in the GI tract at day two post-infection that reside in the cecum and ileum (Figure S8). A resolution from gut bacterial load was observed at day four post-infection, whereby only two out of five mice displayed Kp load in the cecum and colon that was above detection limit (Figure S8). Importantly, we could detect a high Kp load in the esophagus of short needle gavage mice at day two post-infection with similar Kp load resolution at day four post-infection (Figure 7B). Interestingly, Kp was also recovered from the nasal flush of mice infected with hvKp through short needle gavage at day two post-infection (Figure 7C). In addition, in mice infected with hvKp via intranasal or intratracheal routes, the detection of Kp in the esophagus at 12h post-infection (Figure 7D) preceded the detection of Kp in other parts of the GI tract at 24h post-infection (Figure 5D; Figure S4). Taken together, the data support the notion that early esophagus infection is crucial in establishing downstream intestinal colonization with hvKp.

## DISCUSSION

The colonization and invasion of mucosal surfaces served as a crucial reservoir and the point of entry for pathogenic Kp infection.<sup>38,46</sup> Many studies have approached the understanding of infection pathogenesis from the bacterial perspective. Crucial Kp virulence factors such as capsule, lipopolysaccharide, siderophore, and pili (Riwu K.H.P. et al.<sup>45</sup>) have been identified. However, the mechanism of interaction between

Kp and the host mucosal surface through these different virulence factors remains largely unknown. Infection models that can incorporate the complexity of the mucosal compositions, which include microbiota, mucus, and mucosal immunity will bolster the study of Kp colonization and infection.

*In vivo* mice infection models are excellent system that can capture the complexity of the mucosal tissue. However, two factors should be adequately addressed when applying them in Kp pathogenesis studies. Firstly, there are currently no standard predictive animal models for Kp infection. Many models relied on infection conditions that poorly reflect natural infections, such as antibiotic or chemical pre-treatment, invasive inoculation routes or unrealistically high infection dose ( $>10^8$  CFU), to establish pathogenic infection in mice.<sup>42</sup> In addition, mice are more susceptible to symptomatic hvKp than cKp infection, leading to a bias of *in vivo* virulence studies being conducted with hvKp. The outcomes and observations from these studies may not be directly applicable to cKp. Secondly, the clinically dominant Kp clones of interest are distinct geographically and their independent evolution makes phenotypic comparison of clinical studies across regions complex.

In this study, we tackled these two issues by conducting comparative *in vivo* infection by developing murine models of cKp and hvKp that do not require antibiotic pre-treatment and that mimic the natural route of infection through the different mucosal membranes of the respiratory tract and GI tract. An emphasis was placed on the bacterial tropism in the different mucosal membranes, which remains poorly elucidated in patients due to the absence of clinical biopsy or postmortem reports.

Our study revealed highly differential mucosal tropism between cKp and hvKp infections. In cKp infection, the early infection of the nasal cavity and nasopharynx is critical for establishing downstream lung and gut infection in the absence of antibiotic pre-treatment. Within the respiratory tract, a higher proportion of the bacterial load resided and replicated within the nasal cavity, while cKp load rapidly waned in the lungs early in the infection. Such cKp tropism induces a uniform and widespread bronchoalveolar inflammation and bronchopneumonia throughout the lung. Within the GI tract, cKp primarily resided within the cecum and colon but not the small intestine. A greater amount (5–10x) of bacterial load can be seen in the cecum as compared to the colon for both acute and chronic time points. Similar GI tropism in the cecum was reported in an occult ST258 Kp colonization model.<sup>50</sup> Importantly, infection routes that bypass the nasopharynx opening or nasal cavity fail to induce gut colonization. Once colonization is established, they persist chronically and asymptotically. Interestingly, this gut colonization by cKp in the mouse mirrors observation from longitudinal Kp cohorts where lineage-matched Kp can be isolated from rectal swab or feces across various time points.<sup>41,51,52</sup> Together, these led to the postulation that cKp may undergo *in vivo* “adaptation” during early infection events in the nasal cavity. This enables the cKp to displace existing commensal and establish itself within a niche of the lower intestinal tract at a low dose to avoid inducing protective host responses, thus allowing chronic fecal shedding that supports its infection cycle. Further experimental work will be required to validate or dismiss this postulate.

The first hint of the importance of nasal cavity in cKp pathogenesis was shown clinically, where colonization rate of the nasopharynx was reported to be 3–15%.<sup>40,53–55</sup> More recently, a surveillance study conducted in an ICU showed that nasal Kp can be recovered from patients who acquired fresh colonization in the ICU, while rectal Kp was only recovered from patients with Kp colonization prior to ICU admission.<sup>51</sup> Complementing the role of nasopharyngeal sites in Kp colonization, gastrointestinal colonization was also demonstrated clinically to be a substantial source of hospital-acquired cKp infection.<sup>41,46</sup> Specifically, a greater proportion of hospital-acquired Kp infection occurs within patients that are Kp colonized prior to hospitalization and Gorrie et al. showed that ~49% of such infection could be traced back to the lineage of the colonizing Kp.<sup>41,46</sup>

In hvKp infection, the upper respiratory tract played a lesser role in disease pathogenesis. Unlike cKp, hvKp can replicate efficiently within the lungs, leading to necrotizing foci in the lung periphery that allow the bacteria to spread into the adipose tissue of the mediastinal region. Surprisingly, the fatty area in the lung mediastinal supported a larger hvKp burden than the parenchyma region of the lungs. Consistent with this observation, other studies have shown that high adipose tissue is a predictor of mortality in clinical Kp infection<sup>56</sup> and diet-induced obesity impairs host defense against Kp infection in mice.<sup>57</sup> In the GI tract, a higher proportion of the bacteria were able to reside within the small intestine ileum, suggesting a different niche from cKp. Gut colonization was usually transient despite the higher initial bacterial load (10–100x), suggesting that this high initial bacterial load induce protective host responses that led to clearance. Importantly, *in vivo* adaptation that supports establishment of gut colonization can occur through the esophagus. The concept that the upper GI tract helps to establish hvKp infection in the gut was first proposed in Young et al., in 2020.<sup>48</sup> They compared “oral feeding” with standard gavage and highlighted the importance of oral cavity in supporting hvKp gut colonization. This “oral feeding” inoculation is similar to oral dispense method used in our study, where the inoculum comes in contact with the nasopharynx opening. This could lead to airway infection and confounded experimental conclusion. Our study refined the different oral inoculation methods and provided the precision to define the role of esophagus in the gut infection pathogenesis of hvKp through a “short feeding needle” gavage methodology. Currently, the molecular mechanism on how early esophagus or upper airway infection overcome colonization resistance in the gut remains unknown. We postulate that the contact between bacteria and host cells in these regions could trigger virulence factors regulations that enable these downstream events.

While cKp and hvKp utilize different mucosal tissues to establish downstream gut colonization, an “adaptation” event occurs in the early infection. Different virulence mechanisms exist within different Kp strains that determine the host-pathogen interplay. One possibility is that Kp interactions with the mucosal tissues can trigger bacterial gene expression involved in the survival or pathogenicity of the strain. Similar mechanisms of virulence variation, regulated by different triggers, have been demonstrated in a wide range of bacteria, including *Salmonella enteric*, *Bacillus subtilis*, *Clostridia*, *Listeria monocytogenes*, *Acinetobacter baumannii*, and *Pseudomonas aeruginosa* (Desai S.K. et al.<sup>58</sup>). To the best of our knowledge, this *in vivo* adaptive mechanism has not yet to be described for Kp pathogenesis.

The knowledge generated in this study has implications beyond the understanding of mucosal pathogenesis and can be applied to emerging disciplines related to controlling AMR Kp infections. One such area is the study of microbiome-Kp interactions to enable

application of colonization resistance and decolonization of Kp in the host. The importance of nasal cavity infection as the earliest event required for the establishment of cKp colonization suggests that microbiome diversity in the nasal flush of patients that can block this event should be profiled. Importantly, the absence of antibiotic pre-treatment and chronic colonization of AMR cKp models developed in this study provide a suitable platform for the conduct of microbiome-Kp interaction in the gut. Another area that has gained much momentum is the therapeutic use of bacteriophages in Kp therapy<sup>59</sup> as AMR cKp exhausts antibiotic treatment options. One major concern of such therapy is the occurrence of phage-resistant bacteria that comes with a fitness cost.<sup>60</sup> As such, we hypothesize that the gut could be permissive to the expansion and persistence of phage-resistant Kp due to their immune-suppressed nature. Kp models established in this study allow the killing efficacy testing of phage in the lungs and phage-mutant study in the GI tract *in vivo*.

Together, this study highlights the differential mucosal pathogenesis of dominant cKp and hvKp strains in USA and Asia. Importantly, the methodology and characterization of Kp mucosal infection in this study provide a foundation for mechanistic virulence factors identification and inform novel infection intervention strategies against cKp and hvKp infections.

### Limitations of the study

There are several limitations and important questions that are left unanswered by the design of this study. Firstly, while the bacterial tropism provides the sequence of infection in the mucosal surfaces, the precise mechanism, virulence factors, and host responses that mediate this process are yet to be determined. Secondly, we have focused only on the most pre-dominant cKp (ST258) and hvKp (ST23) for this study. Future studies on other cKp and hvKp should be performed.

### STAR★METHODS

Detailed methods are provided in the online version of this paper and include the following:

- KEY RESOURCES TABLE
- RESOURCE AVAILABILITY
  - Lead contact
  - Materials availability
  - Data and code availability
- EXPERIMENTAL MODEL AND SUBJECT DETAILS
  - Mice
  - Pathogens strains
- METHOD DETAILS
  - Molecular characterization of Kp isolates
  - Quantification of bacterial load
  - Production of *in vivo* infection stock of bacteria
  - Preparation of *in vivo* infection stocks
  - Mucoviscosity assay
  - Intranasal infection
  - Intratracheal infection
  - Oral infection methods
  - Quantification of faecal Kp load
  - Quantification of Kp load in mouse organs
  - Quantification of Kp load in nasal flush
  - Histology of lungs tissues
  - Immunohistochemistry (IHC) and image analysis
- QUANTIFICATION AND STATISTICAL ANALYSIS

### SUPPLEMENTAL INFORMATION

Supplemental information can be found online at <https://doi.org/10.1016/j.isci.2024.108875>.

### ACKNOWLEDGMENTS

We thank the staff from A\*STAR ID Labs Mouse Core, Cindy Phuah and Tian Tian Yap for support in animal breeding. We thank Dr. Amanda Bifani for proof reading of this manuscript. We thank Dr. Andrea Kwa and Associate Professor Gan Yunn Hwen for access of clinical Kp isolated from liver abscess patients in Singapore General Hospital and AKLASS study respectively.

This research was funded by the A\*STAR Infectious Diseases Labs core research grants by Biomedical Research Council of Agency for Science, Technology and Research (A\*STAR) and TF IPC Ltd grant titled “Temasek Foundation Infectious Diseases Programme for Surveillance and Diseases X Resilience”. This research was also supported by the Young Individual Research Grant (OFYIRG22jul-0042) by the National

Medical Research Council, and a grant (BNK and LC) from the National Institutes of Health (R01AI090155). Jun Hao Liew is supported by an A\*STAR Graduate Scholarship. The funders had no role in the study design, data collection or analysis, decision to publish, or preparation of the manuscript.

### AUTHOR CONTRIBUTIONS

Conceptualization and methodology, P.B. and T.H.T.; Investigation, T.H.T., N.N.A., M.Y., J.H.L., J.Q.C., N.K., R.R., and L.C.; Formal analysis, T.H.T. and L.C.; Writing – original draft, P.B. and T.H.T.; Writing – review and editing, R.R., L.C., and B.N.K.; Funding acquisition, P.B., T.H.T., L.C., and B.N.K.; Resources, P.B. and B.N.K.; Supervision, P.B.

### DECLARATION OF INTERESTS

All authors declare no conflicts of interest.

Received: June 2, 2023

Revised: September 28, 2023

Accepted: January 8, 2024

Published: January 11, 2024

### REFERENCES

- Jonas, O.B., Irwin, A., Berthe, F.C.J., Le Gall, F.G., and Marquez, P.V. (2017). Drug-Resistant Infections: A Threat to Our Economic Future (World Bank Group).
- Antimicrobial Resistance Collaborators (2022). Global burden of bacterial antimicrobial resistance in 2019: a systematic analysis. *Lancet* 399, 629–655.
- van Duin, D., Arias, C.A., Komarow, L., Chen, L., Hanson, B.M., Weston, G., Cober, E., Garner, O.B., Jacob, J.T., Satlin, M.J., et al. (2020). Molecular and clinical epidemiology of carbapenem-resistant Enterobacteriales in the USA (CRACKLE-2): a prospective cohort study. *Lancet Infect. Dis.* 20, 731–741.
- Xu, Y., Gu, B., Huang, M., Liu, H., Xu, T., Xia, W., and Wang, T. (2015). Epidemiology of carbapenem resistant Enterobacteriaceae (CRE) during 2000–2012 in Asia. *J. Thorac. Dis.* 7, 376–385.
- Liu, Y.C., Cheng, D.L., and Lin, C.L. (1986). Klebsiella pneumoniae liver abscess associated with septic endophthalmitis. *Arch. Intern. Med.* 146, 1913–1916.
- Dai, P., and Hu, D. (2022). The making of hypervirulent Klebsiella pneumoniae. *J. Clin. Lab. Anal.* 36, e24743.
- Wyres, K.L., and Holt, K.E. (2016). Klebsiella pneumoniae Population Genomics and Antimicrobial-Resistant Clones. *Trends Microbiol.* 24, 944–956.
- Wyres, K.L., Lam, M.M.C., and Holt, K.E. (2020). Population genomics of Klebsiella pneumoniae. *Nat. Rev. Microbiol.* 18, 344–359.
- Zhang, R., Liu, L., Zhou, H., Chan, E.W., Li, J., Fang, Y., Li, Y., Liao, K., and Chen, S. (2017). Nationwide Surveillance of Clinical Carbapenem-resistant Enterobacteriaceae (CRE) Strains in China. *EBioMedicine* 19, 98–106.
- Chiu, S.K., Ma, L., Chan, M.C., Lin, Y.T., Fung, C.P., Wu, T.L., Chuang, Y.C., Lu, P.L., Wang, J.T., Lin, J.C., and Yeh, K.M. (2018). Carbapenem Nonsusceptible Klebsiella pneumoniae in Taiwan: Dissemination and Increasing Resistance of Carbapenemase Producers During 2012–2015. *Sci. Rep.* 8, 8468.
- Marimuthu, K., Venkatachalam, I., Koh, V., Harbarth, S., Perencevich, E., Cherng, B.P.Z., Fong, R.K.C., Pada, S.K., Ooi, S.T., Smitasin, N., et al. (2022). Whole genome sequencing reveals hidden transmission of carbapenemase-producing Enterobacteriales. *Nat. Commun.* 13, 3052.
- Yoon, E.J., Kim, J.O., Kim, D., Lee, H., Yang, J.W., Lee, K.J., and Jeong, S.H. (2018). Klebsiella pneumoniae Carbapenemase Producers in South Korea between 2013 and 2015. *Front. Microbiol.* 9, 56.
- Takeuchi, D., Kerdsin, A., Akeda, Y., Sugawara, Y., Sakamoto, N., Matsumoto, Y., Motooka, D., Ishihara, T., Nishi, I., Laolerd, W., et al. (2022). Nationwide surveillance in Thailand revealed genotype-dependent dissemination of carbapenem-resistant Enterobacteriales. *Microb. Genom.* 8, 000797.
- Zhang, Y., Zhao, C., Wang, Q., Wang, X., Chen, H., Li, H., Zhang, F., Li, S., Wang, R., and Wang, H. (2016). High Prevalence of Hypervirulent Klebsiella pneumoniae Infection in China: Geographic Distribution, Clinical Characteristics, and Antimicrobial Resistance. *Antimicrob. Agents Chemother.* 60, 6115–6120.
- Wyres, K.L., Nguyen, T.N.T., Lam, M.M.C., Judd, L.M., van Vinh Chau, N., Dance, D.A.B., Ip, M., Karkey, A., Ling, C.L., Miliya, T., et al. (2020). Genomic surveillance for hypervirulence and multi-drug resistance in invasive Klebsiella pneumoniae from South and Southeast Asia. *Genome Med.* 12, 11.
- Lee, C.R., Lee, J.H., Park, K.S., Jeon, J.H., Kim, Y.B., Cha, C.J., Jeong, B.C., and Lee, S.H. (2017). Antimicrobial Resistance of Hypervirulent Klebsiella pneumoniae: Epidemiology, Hypervirulence-Associated Determinants, and Resistance Mechanisms. *Front. Cell. Infect. Microbiol.* 7, 483.
- Liao, W., Li, D., Liu, F., Du, F.L., Long, D., Zhang, W., and Liu, Y. (2020). Distribution of integrons and phylogenetic groups among highly virulent serotypes of Klebsiella pneumoniae in a Chinese tertiary hospital. *J. Glob. Antimicrob. Resist.* 21, 278–284.
- Shi, Q., Quan, J., Lan, P., Huang, D., Zhou, J., Jiang, Y., and Yu, Y. (2020). Prevalence and characteristics of pks gene cluster harbouring Klebsiella pneumoniae from bloodstream infection in China. *Epidemiol. Infect.* 148, e69.
- Gao, Q., Shen, Z., Qin, J., Liu, Y., and Li, M. (2020). Antimicrobial Resistance and Pathogenicity Determination of Community-Acquired Hypervirulent Klebsiella pneumoniae. *Microb. Drug Resist.* 26, 1195–1200.
- Li, L., Yuan, Z., Chen, D., Xie, X., and Zhang, B. (2020). Clinical and Microbiological Characteristics of Invasive and Hypervirulent Klebsiella pneumoniae Infections in a Teaching Hospital in China. *Infect. Drug Resist.* 13, 4395–4403.
- Sanikhani, R., Moeinirad, M., Shahcheraghi, F., Lari, A., Fereshteh, S., Sepehr, A., Salimi, A., and Badmasti, F. (2021). Molecular epidemiology of hypervirulent Klebsiella pneumoniae: a systematic review and meta-analysis. *Iran. J. Microbiol.* 13, 257–265.
- Siu, L.K., Fung, C.P., Chang, F.Y., Lee, N., Yeh, K.M., Koh, T.H., and Ip, M. (2011). Molecular typing and virulence analysis of serotype K1 Klebsiella pneumoniae strains isolated from liver abscess patients and stool samples from noninfectious subjects in Hong Kong, Singapore, and Taiwan. *J. Clin. Microbiol.* 49, 3761–3765.
- Lin, J.C., Koh, T.H., Lee, N., Fung, C.P., Chang, F.Y., Tsai, Y.K., Ip, M., and Siu, L.K. (2014). Genotypes and virulence in serotype K2 Klebsiella pneumoniae from liver abscess and non-infectious carriers in Hong Kong, Singapore and Taiwan. *Gut Pathog.* 6, 21.
- Wyres, K.L., Wick, R.R., Judd, L.M., Froumine, R., Tokolyi, A., Gorrie, C.L., Lam, M.M.C., Duchêne, S., Jenney, A., and Holt, K.E. (2019). Distinct evolutionary dynamics of horizontal gene transfer in drug resistant and virulent clones of Klebsiella pneumoniae. *PLoS Genet.* 15, e1008114.
- Lee, I.R., Molton, J.S., Wyres, K.L., Gorrie, C., Wong, J., Hoh, C.H., Teo, J., Kalimuddin, S., Lye, D.C., Archuleta, S., et al. (2016). Differential host susceptibility and bacterial virulence factors driving Klebsiella liver abscess in an ethnically diverse population. *Sci. Rep.* 6, 29316.
- De Francesco, M.A., Tiecco, G., Scaltriti, E., Piccinelli, G., Corbellini, S., Gurrieri, F., Crosato, V., Moiola, G., Marchese, V., Focà, E., et al. (2023). First Italian report of a liver abscess and metastatic endogenous endophthalmitis caused by ST-23 hypervirulent Klebsiella pneumoniae in an immunocompetent individual. *Infection* 51, 271–276.

27. Fliss, M., van den Berg, C.H.S.B., Kuijper, E., Notermans, D.W., Hendrickx, A.P.A., Schoots, M.H., and Bathoorn, E. (2022). Brief report: community-acquired Friedlander's pneumonia and pulmonary metastatic *Klebsiella pneumoniae* infection caused by hypervirulent ST23 in the Netherlands. *Eur. J. Clin. Microbiol. Infect. Dis.* *41*, 1133–1138.
28. Anantharajah, A., Deltombe, M., de Barys, M., Evrard, S., Denis, O., Bogaerts, P., Hallin, M., Miendje Deyi, V.Y., Pierard, D., Bruynseels, P., et al. (2022). Characterization of hypervirulent *Klebsiella pneumoniae* isolates in Belgium. *Eur. J. Clin. Microbiol. Infect. Dis.* *41*, 859–865.
29. Hernández, M., López-Urrutia, L., Abad, D., De Frutos Serna, M., Ocampo-Sosa, A.A., and Eiros, J.M. (2021). First Report of an Extensively Drug-Resistant ST23 *Klebsiella pneumoniae* of Capsular Serotype K1 Co-Producing CTX-M-15, OXA-48 and ArmA in Spain. *Antibiotics* *10*, 157.
30. Rafat, C., Messia, J., Barnaud, G., Dufour, N., Magdoud, F., Billard-Pomares, T., Gaudry, S., Dreyfuss, D., Branger, C., Decré, D., and Ricard, J.D. (2018). Hypervirulent *Klebsiella pneumoniae*, a 5-year study in a French ICU. *J. Med. Microbiol.* *67*, 1083–1089.
31. Becker, L., Kaase, M., Pfeifer, Y., Fuchs, S., Reuss, A., von Laer, A., Sin, M.A., Korte-Berwanger, M., Gatermann, S., and Werner, G. (2018). Genome-based analysis of Carbapenemase-producing *Klebsiella pneumoniae* isolates from German hospital patients, 2008–2014. *Antimicrob. Resist. Infect. Control* *7*, 62.
32. Pereira, A., Petrucci, T., and Simões, M.J. (2017). [*Klebsiella pneumoniae* from K1 and Hypervirulent Clone ST23: First Documented Case in Portugal]. *Acta Med. Port.* *30*, 496–499.
33. Cubero, M., Grau, I., Tubau, F., Pallarés, R., Dominguez, M.A., Liñares, J., and Ardanuy, C. (2016). Hypervirulent *Klebsiella pneumoniae* clones causing bacteraemia in adults in a teaching hospital in Barcelona, Spain (2007–2013). *Clin. Microbiol. Infect.* *22*, 154–160.
34. Lam, M.M.C., Wick, R.R., Watts, S.C., Cerdeira, L.T., Wyres, K.L., and Holt, K.E. (2021). A genomic surveillance framework and genotyping tool for *Klebsiella pneumoniae* and its related species complex. *Nat. Commun.* *12*, 4188.
35. Zeng, L., Deng, Q., Zeng, T., Liu, Y., Zhang, J., and Cao, X. (2020). Prevalence of Carbapenem-Resistant *Klebsiella pneumoniae* Infection in Southern China: Clinical Characteristics, Antimicrobial Resistance, Virulence, and Geographic Distribution. *Microb. Drug Resist.* *26*, 483–491.
36. Cheong, H.S., Chung, D.R., Park, M., Kim, S.H., Ko, K.S., Ha, Y.E., Kang, C.I., Peck, K.R., and Song, J.H. (2017). Emergence of an extended-spectrum beta-lactamase-producing serotype K1 *Klebsiella pneumoniae* ST23 strain from Asian countries. *Epidemiol. Infect.* *145*, 990–994.
37. Fuxench-López, Z., and Ramírez-Ronda, C.H. (1978). Pharyngeal flora in ambulatory alcoholic patients: prevalence of gram-negative bacilli. *Arch. Intern. Med.* *138*, 1815–1816.
38. Podschun, R., and Ullmann, U. (1998). *Klebsiella* spp. as nosocomial pathogens: epidemiology, taxonomy, typing methods, and pathogenicity factors. *Clin. Microbiol. Rev.* *11*, 589–603.
39. Pollack, M., Charache, P., Nieman, R.E., Jett, M.P., Reimhardt, J.A., and Hardy, P.H., Jr. (1972). Factors influencing colonisation and antibiotic-resistance patterns of gram-negative bacteria in hospital patients. *Lancet* *2*, 668–671.
40. Dao, T.T., Liebenthal, D., Tran, T.K., Ngoc Thi Vu, B., Ngoc Thi Nguyen, D., Thi Tran, H.K., Thi Nguyen, C.K., Thi Vu, H.L., Fox, A., Horby, P., et al. (2014). *Klebsiella pneumoniae* oropharyngeal carriage in rural and urban Vietnam and the effect of alcohol consumption. *PLoS One* *9*, e91999.
41. Gorrie, C.L., Mirceta, M., Wick, R.R., Edwards, D.J., Thomson, N.R., Strugnelli, R.A., Pratt, N.F., Garlick, J.S., Watson, K.M., Pilcher, D.V., et al. (2017). Gastrointestinal Carriage Is a Major Reservoir of *Klebsiella pneumoniae* Infection in Intensive Care Patients. *Clin. Infect. Dis.* *65*, 208–215.
42. Joseph, L., Merciecca, T., Forestier, C., Balestrino, D., and Miquel, S. (2021). From *Klebsiella pneumoniae* Colonization to Dissemination: An Overview of Studies Implementing Murine Models. *Microorganisms* *9*, 1282.
43. Wong Fok Lung, T., Charytonowicz, D., Beaumont, K.G., Shah, S.S., Sridhar, S.H., Gorrie, C.L., Mu, A., Hofstaedter, C.E., Varisco, D., McConville, T.H., et al. (2022). *Klebsiella pneumoniae* induces host metabolic stress that promotes tolerance to pulmonary infection. *Cell Metabol.* *34*, 761–774.e9.
44. Lam, M.M.C., Wyres, K.L., Duchêne, S., Wick, R.R., Judd, L.M., Gan, Y.H., Hoh, C.H., Archuleta, S., Molton, J.S., Kalimuddin, S., et al. (2018). Population genomics of hypervirulent *Klebsiella pneumoniae* clonal-group 23 reveals early emergence and rapid global dissemination. *Nat. Commun.* *9*, 2703.
45. Palacios, M., Miner, T.A., Frederick, D.R., Sepulveda, V.E., Quinn, J.D., Walker, K.A., and Miller, V.L. (2018). Identification of Two Regulators of Virulence That Are Conserved in *Klebsiella pneumoniae* Classical and Hypervirulent Strains. *mBio* *9*, e01443-18.
46. Martin, R.M., Cao, J., Brisse, S., Passet, V., Wu, W., Zhao, L., Malani, P.N., Rao, K., and Bachman, M.A. (2016). Molecular Epidemiology of Colonizing and Infecting Isolates of *Klebsiella pneumoniae*. *mSphere* *1*, e00261-16.
47. Viau, R.A., Hujer, A.M., Marshall, S.H., Perez, F., Hujer, K.M., Briceño, D.F., Dul, M., Jacobs, M.R., Grossberg, R., Toltzis, P., and Bonomo, R.A. (2012). "Silent" dissemination of *Klebsiella pneumoniae* isolates bearing K. pneumoniae carbapenemase in a long-term care facility for children and young adults in Northeast Ohio. *Clin. Infect. Dis.* *54*, 1314–1321.
48. Young, T.M., Bray, A.S., Nagpal, R.K., Caudell, D.L., Yadav, H., and Zafar, M.A. (2020). Animal Model To Study *Klebsiella pneumoniae* Gastrointestinal Colonization and Host-to-Host Transmission. *Infect. Immun.* *88*, e00071-20.
49. Riwu, K.H.P., Effendi, M.H., Rantam, F.A., Khairullah, A.R., and Widodo, A. (2022). A review: Virulence factors of *Klebsiella pneumoniae* as emerging infection on the food chain. *Vet. World* *15*, 2172–2179.
50. Sim, C.K., Kashaf, S.S., Stacy, A., Proctor, D.M., Almeida, A., Bouladoux, N., Chen, M., NISC Comparative Sequencing Program, Finn, R.D., Belkaid, Y., et al. (2022). A mouse model of occult intestinal colonization demonstrating antibiotic-induced outgrowth of carbapenem-resistant Enterobacteriaceae. *Microbiome* *10*, 43.
51. Thuy, D.B., Campbell, J., Thuy, C.T., Hoang, N.V.M., Voong Vinh, P., Nguyen, T.N.T., Nguyen Ngoc Minh, C., Pham, D.T., Rabaa, M.A., Lan, N.P.H., et al. (2021). Colonization with *Staphylococcus aureus* and *Klebsiella pneumoniae* causes infections in a Vietnamese intensive care unit. *Microb. Genom.* *7*, 000514.
52. Qin, X., Wu, S., Hao, M., Zhu, J., Ding, B., Yang, Y., Xu, X., Wang, M., Yang, F., and Hu, F. (2020). The Colonization of Carbapenem-Resistant *Klebsiella pneumoniae*: Epidemiology, Resistance Mechanisms, and Risk Factors in Patients Admitted to Intensive Care Units in China. *J. Infect. Dis.* *221*, S206–S214.
53. Davis, T.J., and Matsen, J.M. (1974). Prevalence and characteristics of *Klebsiella* species: relation to association with a hospital environment. *J. Infect. Dis.* *130*, 402–405.
54. Wolf, B., Rey, L.C., Moreira, L.B., Milatovic, D., Fleer, A., Verhoef, J., and Roord, J.J. (2001). Carriage of gram-negative bacilli in young Brazilian children with community-acquired pneumonia. *Int. J. Infect. Dis.* *5*, 155–159.
55. Farida, H., Severin, J.A., Gasem, M.H., Keuter, M., van den Broek, P., Hermans, P.W.M., Wahyono, H., and Verbrugh, H.A. (2013). Nasopharyngeal carriage of *Klebsiella pneumoniae* and other Gram-negative bacilli in pneumonia-prone age groups in Semarang, Indonesia. *J. Clin. Microbiol.* *51*, 1614–1616.
56. Ying, P., Chen, J., Ye, Y., Ye, J., and Cai, W. (2022). Adipose tissue is a predictor of 30-days mortality in patients with bloodstream infection caused by carbapenem-resistant *Klebsiella pneumoniae*. *BMC Infect. Dis.* *22*, 173.
57. Mancuso, P., Curtis, J.L., Weitzel, A.M., Griffin, C.A., Bouchard, B., Freeman, C.M., Bridges, D., and Singer, K. (2022). Diet-induced obesity in mice impairs host defense against *Klebsiella pneumoniae* in vivo and glucose transport and bactericidal functions in neutrophils in vitro. *Am. J. Physiol. Lung Cell Mol. Physiol.* *322*, L116–L128.
58. Desai, S.K., and Kenney, L.J. (2019). Switching Lifestyles Is an in vivo Adaptive Strategy of Bacterial Pathogens. *Front. Cell. Infect. Microbiol.* *9*, 421.
59. Turner, P.V., Pekow, C., Vasbinder, M.A., and Brabb, T. (2011). Administration of substances to laboratory animals: equipment considerations, vehicle selection, and solute preparation. *J. Am. Assoc. Lab. Anim. Sci.* *50*, 614–627.
60. Oechslin, F. (2018). Resistance Development to Bacteriophages Occurring during Bacteriophage Therapy. *Viruses* *10*.
61. Satlin, M.J., Chen, L., Gomez-Simmonds, A., Marino, J., Weston, G., Bhowmik, T., Seo, S.K., Sperber, S.J., Kim, A.C., Eilertson, B., et al. (2022). Impact of a Rapid Molecular Test for *Klebsiella pneumoniae* Carbapenemase and Ceftazidime-Avibactam Use on Outcomes After Bacteremia Caused by Carbapenem-Resistant Enterobacteriales. *Clin. Infect. Dis.* *75*, 2066–2075.
62. Satlin, M.J., Chen, L., Patel, G., Gomez-Simmonds, A., Weston, G., Kim, A.C., Seo, S.K., Rosenthal, M.E., Sperber, S.J., Jenkins, S.G., et al. (2017). Multicenter Clinical and

- Molecular Epidemiological Analysis of Bacteremia Due to Carbapenem-Resistant Enterobacteriaceae (CRE) in the CRE Epicenter of the United States. *Antimicrob. Agents Chemother.* *61*, e02349-16.
63. Molton, J., Phillips, R., Gandhi, M., Yoong, J., Lye, D., Tan, T.T., Fisher, D., and Archuleta, S. (2013). Oral versus intravenous antibiotics for patients with *Klebsiella pneumoniae* liver abscess: study protocol for a randomized controlled trial. *Trials* *14*, 364.
64. Feldgarden, M., Brover, V., Gonzalez-Escalona, N., Frye, J.G., Haendiges, J., Haft, D.H., Hoffmann, M., Pettengill, J.B., Prasad, A.B., Tillman, G.E., et al. (2021). AMRFinderPlus and the Reference Gene Catalog facilitate examination of the genomic links among antimicrobial resistance, stress response, and virulence. *Sci. Rep.* *11*, 12728.
65. Lam, M.M.C., Wick, R.R., Judd, L.M., Holt, K.E., and Wyres, K.L. (2022). Kaptive 2.0: updated capsule and lipopolysaccharide locus typing for the *Klebsiella pneumoniae* species complex. *Microb. Genom.* *8*, 000800.
66. Teo, T.H., Chan, Y.H., Lee, W.W.L., Lum, F.M., Amrun, S.N., Her, Z., Rajarethinam, R., Merits, A., Röttschke, O., Rénia, L., and Ng, L.F.P. (2017). Fingolimod treatment abrogates chikungunya virus-induced arthralgia. *Sci. Transl. Med.* *9*, eaal1333.

## STAR★METHODS

### KEY RESOURCES TABLE

REAGENT or RESOURCE	SOURCE	IDENTIFIER
<b>Antibodies</b>		
Anti-Klebsiella pneumoniae polyclonal antibody	ThermoFisher Scientific	AB_559816
DISCOVERY OmniMap anti-Rb HRP	Roche	Cat# 760-4311
ChromoMap DAB kit	Roche	Cat# 760-159
<b>Bacterial and virus strains</b>		
Classical Klebsiella pneumoniae strain 1085 (ST258)	SAMN27308114	Kp1085
Classical Klebsiella pneumoniae strain 1050 (ST258)	SAMN06218025	Kp1050
Classical Klebsiella pneumoniae strain 1055 (ST258)	SAMN06218036	Kp1055
Classical Klebsiella pneumoniae strain 1054 (ST258)	SAMN06218040	Kp1054
Classical Klebsiella pneumoniae strain 1064 (ST258)	SAMN06218124	Kp1064
Hypervirulent Klebsiella pneumoniae strain 0675 (ST23)	SAMN38717950	KpEC0675
Hypervirulent Klebsiella pneumoniae strain SGH10 (ST23)	SAMN06112188	KpSGH10
Hypervirulent Klebsiella pneumoniae strain NUH27 (ST23)	SAMN38717951	KpNUH27
<b>Chemicals, peptides, and recombinant proteins</b>		
Carbenicillin disodium salt	Sigma-Aldrich	C1389
LB Broth Miller	1 <sup>st</sup> Base	BIO-4000-1kg
LB Agar Miller	1 <sup>st</sup> Base	BIO-4010-1kg
<b>Deposited data</b>		
WGS data of KpEC0675 was newly generated in this study and deposited into NCBI GeneBank database	Accession: SAMN38717950	KpEC0675
WGS data of KpNUH27 was newly generated in this study and deposited into NCBI GeneBank database	Accession: SAMN38717951	KpNUH27
<b>Experimental models: Organisms/strains</b>		
C57BL/6J	The Jackson Laboratory	Stock No: 000664
<b>Software and algorithms</b>		
Prism 9	GraphPad	Version 9.4.1
Kleborate software	<a href="https://github.com/tseemann/snippy">https://github.com/tseemann/snippy</a>	V 4.6.0
Snippy		
AMRFinderPlus		V 3.11.4
Blast		V 2.13

## RESOURCE AVAILABILITY

### Lead contact

Further information and requests for resources and reagents should be directed to and will be fulfilled by the [lead contact](#), Pablo Bifani ([Pablo\\_bifani@IDLabs.a-star.edu.sg](mailto:Pablo_bifani@IDLabs.a-star.edu.sg)).

### Materials availability

This study did not generate new unique reagents. There is restriction to the availability of the *Klebsiella* clinical isolates used in this study because they were provided to the research team under MTA or Research collaboration agreement (RCA) that restrict distribution of the bacteria, but we can guide you to the proper contact.

### Data and code availability

WGS data of ST258, which include Kp1085 (Accession: SAMN27308114), Kp1050 (Accession: SAMN06218025), Kp1055 (Accession: SAMN06218036), Kp1054 (Accession: SAMN06218040) and Kp1064 (Accession: SAMN06218124) used in this study is part of the cohorts collected in 2 different study by Satlin et al.<sup>61,62</sup> WGS data of KpSGH10 (Accession: SAMN06112188) is extracted from AKLASS cohort as part of the study by Lee et al.<sup>25</sup> WGS data of KpEC0675 (Accession: SAMN38717950) and KpNUH27 (Accession: SAMN38717951) have been deposited in NCBI GeneBank database and are publicly available as of the date of publication. Biosample numbers are listed in the [key resources table](#).

This paper does not report original code.

Any additional information required to reanalyse the data reported in this paper is available from the [lead contact](#) upon request.

## EXPERIMENTAL MODEL AND SUBJECT DETAILS

### Mice

Male and female C57BL/6J mice (aged 6 - 10 weeks) in wild-type background were used. All mice were bred and housed under specific pathogen-free conditions in the Biological Resource Centre, Agency for Science, Technology and Research, Singapore. Animals are assigned to control or experimental groups randomly. All experiments and procedures were approved by the Institutional Animal Care and Use Committee (IACUC: 191491) of the Agency for Science, Technology and Research, Singapore, in accordance with the guidelines of the Agri-Food and Veterinary Authority and the National Advisory Committee for Laboratory Animal Research of Singapore.

### Pathogens strains

The clinical isolates of classical ST258 Kp used in this study include Kp1085 (K-locus 107), Kp1050 (K-locus 107), Kp1054 (KL106), Kp2064 (KL106) and Kp1055 (K-locus 23). These isolates were collected from multicentre epidemiological surveillance studies of bacteraemia due to Carbapenem-Resistant Enterobacteriaceae (CRE) in the New York and New Jersey hospitals. All classical Kp used in this study are multi-drug resistant (MDR) and carbapenem resistant isolates.

The clinical isolates of hvKp includes KpEC0675 (K-locus 1), KpSGH10 (K-locus 1) and KpNUH27 (K-locus 1). All hvKp are Asian isolates isolated in the hospitals of Singapore. KpEC0675 and KpSGH10 were isolated in Singapore General Hospital (SGH). KpNUH27 was isolated in National University Hospital (NUH). Both KpSGH10 and KpNUH27 is collected as part of a multicentre trial, Antibiotics for Klebsiella liver abscess study (AKLASS).<sup>63</sup>

## METHOD DETAILS

### Molecular characterization of Kp isolates

The hypervirulence associated genes, including yersiniabactin (ybt), colibactin (clb), salmochelin (iro), salmochelin (iro), aerobactin (iuc), hypermucoidy (rmpADC, rmpA2) loci, were initially determined using Kleborate v2.3.2,<sup>34</sup> followed by confirmation using blastn analysis. Antimicrobial resistance genes were mined using AMRFinderPlus v3.11.4<sup>64</sup> and Kleborate v2.3.2. Klebsiella capsular type (K locus typing) was conducted using Kaptive v2.0.6.<sup>65</sup> Phylogenetic and core SNP analysis was conducted using a previously described method.<sup>3</sup> Detailed genomic characteristics of the isolates used in this study can be found in [Table S1](#).

### Quantification of bacterial load

All quantification of bacterial load in infection stock or tissues from infected animals were done by bacterial spotting method. Specifically, bacterial suspension was 10x serial diluted ( $10^{-1}$  to  $10^{-10}$ ) using LB broth. 10 $\mu$ l of the bacteria from the respective dilution were then spotted onto a LB agar plate with selection antibiotics (100 $\mu$ g/ml of carbenicillin). The spot was allowed to dry before transferring into a 37°C incubator overnight. Dilutions that display spots count between 5 – 30 will be used for determination of bacterial load in CFU/ml.

### Production of *in vivo* infection stock of bacteria

Bacteria were streaked onto LB agar with selection antibiotics (100 $\mu$ g/ml of carbenicillin). A single colony was selected for expansion in 10ml of LB broth with selection antibiotics (100 $\mu$ g/ml of carbenicillin) in overnight culture at 37°C. All 10ml of overnight culture was transferred into 300ml of LB broth and incubated at 37°C with shaking (250rpm) until harvest at  $\sim$ OD<sub>600</sub>1. Harvested bacteria were span down at 10,000G for 10min and the pellets were pooled and washed in 50ml of sterile PBS. Resultant bacteria are span down again at 10,000G for 10min and re-suspended into a final volume of 3-5ml of sterile 12.5% glycerol/PBS. These bacteria were aliquoted (100 $\mu$ l each) into cryotubes and kept frozen in -80°C. A single tube of frozen aliquot was thawed for determination of bacterial concentration by serial dilution and spotting onto LB agar plate. All stocks are frozen down at a load of  $>10^9$  CFUs/ml

### Preparation of *in vivo* infection stocks

Just before infection, add PBS into the frozen aliquot to make a concentration of  $10^9$  CFU/ml. Perform 10x serial dilution with PBS to achieve the concentration required for the different method of infection.

### Mucoviscosity assay

Mucoviscosity assay was adapted from Palacios et al.<sup>45</sup> Briefly, overnight cultures were adjusted to OD-1. 5ml of the bacteria at OD-1 is span down at 1,000g for 5min and supernatant is collected from the top for OD600 reading. The degree of mucoviscosity is measured as the bacteria that fails to spin down by the sedimentation spin.

### Intranasal infection

A non-invasive intranasal procedure that sufficiently deliver inoculum into the lungs at the point of inoculation (Figure S1) was optimized for this study. All intranasal infections for classical and hypervirulent KP were performed at  $6 \times 10^7$  CFUs and  $1 \times 10^3$  CFUs per mouse respectively. Specifically, mice were first sedated in 1-3% isoflurane for 3-5min. Subsequently, the mouse was lay flat with the back on the surface and the nostril facing up. Use 1 finger to block the mouth, then dispense 30 $\mu$ l of bacteria suspension in parts above the nostril. The natural breathing rhythm will allow uptake of the inoculum. Keep the mouth blocked to allow deeper uptake of inoculum into the lungs until mice show first sign of waking up. Allow mice to be fully awake before repeating process to inoculate a total volume of 60 $\mu$ l.

### Intratracheal infection

A non-invasive intratracheal inoculation through the mouth of the mice that make use of the natural breathing was adapted. This method delivers most of the inoculum into the lungs with a small proportion entering the GI tract (Figure S1). All intratracheal infections for classical and hypervirulent Kp were performed at  $6 \times 10^7$  CFUs and  $1 \times 10^3$  CFUs per mouse respectively. For this procedure to work, mice must first be sufficiently sedated in 1-3% isoflurane that will allow them to stay asleep for 1-2 min to complete the procedure. Once sedated, place the mice in the prone position of the surface, then prop up the head and chest into  $\sim 90^\circ$  position from the surface. Pinch the nose to ensure complete breathing through the mouth. Use a pipette tip to open the mouth and dispense 20 $\mu$ l of inoculum above the tongue towards the back of the throat. Allow the mice to breathe in the inoculum naturally. Keep holding the mice with pinched nose for  $\sim 40$  breath to ensure sufficiently deep uptake of inoculum into the lungs.

### Oral infection methods

3 different modes of oral infections, standard oral gavage, short needle gavage and oral dispense was employed in this study to simulate different pathogen entry point during oral infection (Figure S5). Standard gavage was performed with 1.5 inches 20G feeding needle. This is the standard feeding needle length recommended for adult mice that are  $>20$ G.<sup>59</sup> Mice were restrained by scuffing and 100 $\mu$ l of inoculum was dispensed at the entry point just above the stomach. Short needle gavage was performed with 1-inch 20G feeding needle. Similarly, mice were restrained and 200 $\mu$ l of inoculum was dispensed with the oesophagus as the entry point. Oral dispense was performed on mice that are mildly sedated with 1-3% isoflurane and 20 $\mu$ l of inoculum was dispensed just on top of the tongue. The concentrations of the bacterial inoculum were adjusted accordingly to give the same final CFU count for the different methods.

### Quantification of faecal Kp load

On designated days, approximately 2 fresh faecal pellets were collected from each mouse for Kp quantification. Faecal pellets were weighed and transferred into 2ml homogenization tube with 1mm beads (Precelly, Bertin) containing 1ml of selection medium (LB+100 $\mu$ g/ml of carbenicillin). Subsequently, faecal pellets were homogenized at a setting of 6,800 rpm x 3 cycles, 20s delay using a homogenizer (Precelly Evolution, Bertin). The resultant mixture was span down at 400G for 5min to pellet faecal particulates. 100 $\mu$ l of supernatant that contains the bacterial was aspirated for 10x serial dilution in selection medium (LB+100 $\mu$ g/ml of carbenicillin) and bacterial load quantification was determined by spotting of serial diluted products onto LB Agar (with 100 $\mu$ g/ml of carbenicillin). All bacterial load data was normalized to the weight of the faecal pellets. Control experiments has been done to demonstrate that natural flora in the faecal pellets do not grow in the selection agar (data not shown).

### Quantification of Kp load in mouse organs

Bacterial quantification in the lungs, oesophagus, stomach, duodenum, jejunum, ileum, cecum and colon tissues were performed according to the following protocol. At varying time-points, mice were sacrificed by CO<sub>2</sub> gassing. Immediately post-sacrifice, 400-700 $\mu$ l of blood was aspirated by cardiac puncture to reduce amount of blood in the organs. Subsequently, except of oesophagus, the rest of the tissues were excised and placed into 2ml homogenization tube with 1mm beads (Precelly, Bertin) containing 1ml of selection medium (LB+100 $\mu$ g/ml of carbenicillin). Oesophagus was placed into a 2ml homogenization tube with 0.5ml of selection medium. All tissues were homogenized with a setting of 7,200 rpm, 30s x 3 cycles, 15s delay, 4°C using a homogenizer (Precelly Evolution, Bertin). The resultant mixture was span down at 400G for 5min to pellet tissue particulates. 100 $\mu$ l of supernatant that contains the bacterial was aspirated for 10x serial dilution in selection medium (LB+100 $\mu$ g/ml of carbenicillin) and bacterial load quantification was determined by spotting of serial diluted products onto LB Agar (with 100 $\mu$ g/ml of carbenicillin). All bacterial load data was normalized to the weight of the organ. Control experiments has been done to demonstrate that natural flora in the tissues do not grow on the selection agar (data not shown).

### Quantification of Kp load in nasal flush

The quantification of the bacterial load in the nasal flush was performed as a measurement of Kp load in the nasal cavity. At varying time-points, mice were sacrificed by CO<sub>2</sub> gassing. The jaws of the mice were removed to reveal the nasopharynx opening (Figure S5A). 1ml of EDTA (50µm)/PBS was used to flush the nasal cavity with a 19G needle and collections was made at the nose opening. Collected flush liquid were spun down at 10,000G to pellet bacteria and resuspended in 100µl of selection medium (LB+100µg/ml of carbenicillin) for downstream 10x serial dilution and bacterial quantification by spotting.

### Histology of lungs tissues

Mice were euthanized by perfusion with PBS post anaesthesia. Each lung was inflated with ~1ml of 10% neutral buffered formalin, then placed into 25ml of 10% neutral buffered formalin for fixation (24 – 48hrs). Subsequently, paraffin wax block was made for 5 µm-thick sectioning followed by hematoxylin and eosin (H&E) staining as previously described.<sup>66</sup> Histopathological examination was carried out in a blinded fashion based on the presence of the following parameters in the lungs: congestion, haemorrhage (interstitial, intra alveolar/perivascular), bronchio-loalveolar inflammation, perivascular cuffing/peribronchiolar inflammation, alveolar thickening, vascular thrombosis, alveolar oedema, perivascular oedema, vasculitis, alveolar wall necrosis, alveolar emphysema, steatitis of mediastinal adipose tissue, pleuritis, presence of bacteria in parenchyma and lung periphery. Severity of grading were assigned on the following scale: 1 - minimal; 2 - mild; 3 - moderate, 4 – marked & 5 – severe. Mock (PBS) infected mice were used as negative controls. Detailed histopathological scoring of each mouse can be found in Table S2.

### Immunohistochemistry (IHC) and image analysis

Immunohistochemical staining of Klebsiella in mice lungs was performed. Briefly, unstained sections of lung tissues were baked, dewaxed, and rehydrated before the epitope was retrieved for detection of Klebsiella antigen using pH9 (CC1) solution (950-224, Roche) in Ventana Discovery Ultra System (Roche, Ventana Medical system, USA). Then, rabbit polyclonal  $\alpha$ -Klebsiella antibody (1:2000 dilution; Thermofisher Scientific; PA1-7226) was added to the tissues for 60 minutes. This was followed with addition of DISCOVERY OmniMap anti-Rb HRP (760-4311, Roche) for 16 minutes and by ChromoMap DAB kit (760-159, Roche) for 8 minutes. Finally, the tissues were counter stained with hematoxylin stain (760-2208, Roche).

### QUANTIFICATION AND STATISTICAL ANALYSIS

All graphs with bacterial load were presented in Log<sub>10</sub> scale. As a result, data were presented as “CFUs+1” and data with CFUs below detection limit is assigned a value of “1” and appears on the axis of the graphs. All faecal and organ bacterial load were normalised to the weight of the organ and this measurement reflects the bacterial density.

Statistical analyses were performed according to nonparametric distribution of the data using Prism 9 (GraphPad Software). All pair-wise comparison was performed using Mann’s Whitney 2 tailed analysis. All analysis that are 3 groups and above were performed using Kruskal-Wallis test with Dunn’s multiple comparisons. All mortality analysis was performed using Log-rank (Mantel-Cox) test. P values <0.05 were considered statistically significant.